A Power Transmission Design for an Untethered Hydraulic Ankle Orthosis

A THESIS
SUBMITTED TO THE FACULTY OF THE GRADUATE SCHOOL
OF THE UNIVERSITY OF MINNESOTA
BY

Katherine L. Houle

IN PARTIAL FULFILLMENT OF THE REQUIREMENTS
FOR THE DEGREE OF
MASTER OF SCIENCE

WILLIAM K DURFEE

October, 2012

Acknowledgements

I would first like to thank the NSF ERC program and the Center for Compact, Efficient Fluid Power under the direction of Professor Kim Stelson for their financial support during the course of my program. Without this assistance, this opportunity would not have been possible.

The Center for Compact, Efficient Fluid Power not only provided for me financially, but also personally and technically. I am grateful for all the helpful staff of the Center who was willing to assist me in a variety of ways, from clearing up funding issues to sorting out travel accommodations. Don Haney, Alyssa Burger, and Lisa Wissbaum are behind the scenes making sure everything runs smoothly.

I am indebted to the students and subject matter experts of the Center as well. Without the help and guidance offered by them my knowledge of fluid power and the fluid power industry would not have grown as exponentially as it did. I thank Henry Kohring especially for his friendship and vast knowledge.

I would be amiss not to thank my advisor, William Durfee, for all his support, advice, and mentorship. It has been a pleasure to work under an advisor who values hard work and independent, critical thinking, as well as being supportive and offering advice and guidance where needed.

I also thank Professor Liz Hsaio-Wecksler and the Test Bed 6 team of the Center for Compact, Efficient Fluid Power for their support of the project and their collaboration.

I am grateful to Jicheng Xia for being a great mentor to me on this project as well. He is knowledgeable and always willing to take time to help me work through my questions so I can come to a better understanding of the topic at hand. His friendship has been invaluable, and his dedication to his family has been inspiring. All the students of the Durfee Lab have been open and accepting, and my work would not have been as

enjoyable without their company and support.

Finally, I thank my parents, sister, and wonderful husband. Knowing that I have their constant love and support has given me the encouragement and motivation to keep going even in moments of absolute frustration.

The Lord God has been the true giver of all blessings in my life and I give all this work back to Him in thanksgiving for my life and this opportunity.

Abstract

Introduction- Ankle-Foot Orthoses (AFO) can offer assistance to people who have impaired gait due to lower limb and ankle impairments. A powered AFO would fully replace ankle function. A powered AFO should be lightweight, compact and untethered. An hydraulic power transmission design for an AFO has been proposed. The hydraulic power transmission design consists of a battery, a DC motor, a piston pump, a double acting cylinder, and a moment arm acting at the ankle. Methods- The Hydraulic Ankle Foot Orthosis (HAFO) was designed with a method that works from ankle kinetics through each component's "across variables" and "through variables". The HAFO analysis was performed using a complimentary approach allowing for comparison component sizing. A longer moment arm at the ankle required a higher fluid flow rate and cylinder shaft speed but allows for lower system pressure and motor torque. The HAFO was analyzed with a model using an object-oriented approach that allows for manipulation of component parameters to better understand system behavior and efficiency. This simulated analysis was augmented and authenticated by a hardware prototype which provided "real life" parameters for testing the model. The model was used to explore the elements of the transmission design. The hydraulic transmission system's efficiency was affected by component geometry. The system's efficiency increased with a decrease in the cracking pressure of the cap-side check valve and with an increase in cylinder bore diameter. Results- Motors are characteristically high speed and low torque therefore combining a DC motor with a small displacement pump would result in a system with a low flow rate. A lower flow rate results in a small velocity at the ankle. This small velocity allows a small moment arm to be used. However a small moment arm and low pump displacement require a higher motor torque to create the desired force at the ankle. This is the tradeoff of the transmission as power must be conserved within each component. Design Recommendations- The cylinder bore diameter is set at half an inch to keep the system small and compact. Using an achievable motor speed of 6,000 rpm in combination with a pump displacement of 0.4 cc/rev results in a piston velocity of 0.2 m/s. A moment arm of 5 cm with this piston velocity achieves the desired ankle angular velocity. With a 5 cm moment arm and the half-inch cylinder, a motor

torque of 1.2 Nm is needed to achieve maximum ankle torque. Due to this torque, the cylinder and pump will have to withstand 2,000 psi. Most hydraulic equipment is built to withstand at least 2,000 psi. A search did not find any currently available hydraulic cylinders of half-inch diameter or hydraulic piston pumps that operate at 6,000 rpm. These components would have to be customized for the system.

Contents

Acknowledgements **i**

Abstract **iii**

List of Tables **viii**

List of Figures **ix**

1 Introduction **1**

1.1 Ankle-Foot Orthoses 1

1.1.1 Ankle Function and Impairment 2

1.1.2 Passive AFOs 4

1.1.3 Active AFOs 4

1.2 The Hydraulic-powered Ankle-Foot Orthosis 9

1.2.1 Power Transmission Design 11

1.2.2 Research Objective 12

2 Methods **13**

2.1 Mapping Transmission Requirements 13

2.2 Model 17

2.2.1 Dynamics-oriented model 18

2.2.2 Object-oriented model 19

2.2.3 Fluid properties 23

2.2.4 Implementation 23

2.2.5 Model objectives 23

2.3 Model Validation . . . 24
2.4 Parameter determination . . . 26
2.4.1 Motor parameters . . . 26
2.4.2 Pump parameters . . . 27
2.4.3 Cylinder parameters . . . 29
2.5 Data Collection . . . 30
2.6 Model prototype comparison . . . 31

3 Results **32**
3.1 Mapping Ankle Function to Requirements . . . 32
3.2 Dynamic Equations . . . 40
3.3 Determining Component Parameters . . . 42
3.3.1 Pump Parameters . . . 42
3.3.2 Motor Parameters . . . 43
3.3.3 Cylinder Leakage Parameters . . . 45
3.4 Model Validation . . . 47
3.5 Model Exploration . . . 48

4 Discussion **54**
4.1 Design Requirements Method . . . 54
4.2 System Validation . . . 56
4.2.1 Pump Testing . . . 56
4.2.2 Motor Testing . . . 56
4.2.3 Cylinder Leakage . . . 57
4.3 Model Validation . . . 58
4.4 Model Exploration . . . 58
4.5 Design Recommendations . . . 62

5 Conclusion **63**
5.1 General Conclusions . . . 63

References **65**

Appendix A. MATLAB Code for Design Requirements Method **70**

Appendix B. Model Simulation **73**

Appendix C. Datasheets **74**

List of Tables

1.1 A comparison of existing AFO technology described in Section 1.1.3 . . 6
1.2 A comparison of existing exoskeleton and prosthetic technology described in Section 1.1.3 7
2.1 System parameters used in the design requirements method described in Section 2.1 15
2.2 Model parameters described in Section 2.2.2 20
2.3 Component parameters and values used for model validation 27
2.4 Calculated orifice areas 30

List of Figures

1.1 Gait cycle walking illustration 2
1.2 Gait dynamics from Winter 3
1.3 AFO for drop foot 5
1.4 Power transmission design of HAFO 11
2.1 Energy flow through system 14
2.2 Flowchart of component interactions 14
2.3 Model schematic 18
2.4 Photo of the HAFO prototype 25
2.5 Schematic of the hardware prototype 26
2.6 Motor test stand 28
2.7 Pump test stand 28
2.8 HAFO test stand 31
3.1 Ankle dynamics 33
3.2 Piston outputs 34
3.3 Pump outputs 35
3.4 Motor outputs 36
3.5 Battery outputs 37
3.6 Motor outputs comparing pump displacements 38
3.7 Battery outputs comparing motor constants 39
3.8 System pressures 40
3.9 Simulated rod-side pressure with cap-side tank 41
3.10 Simulated rod-side pressure no cap-side relief 42
3.11 Pump pressure-torque curves 43
3.12 Pump flow-speed curves 44

3.13 Pump efficiency 44
3.14 Motor torque-speed 45
3.15 Simulation comparison of piston velocity at 800 rpm 46
3.16 Simulation comparison of piston velocity at 1400 rpm 46
3.17 Simulation comparison of piston velocity at 2000 rpm 46
3.18 Simulation comparison of pressure at 800 rpm 47
3.19 Simulation comparison of pressure at 1400 rpm 47
3.20 Simulation comparison of pressure at 2000 rpm 48
3.21 Model outputs to meet ankle dynamics 49
3.22 Check valve setting effects on the cylinder efficiency 50
3.23 Bore diameter effects on the cylinder efficiency 51
3.24 Pump displacement size effects on system outputs 52
3.25 Bulk modulus effects on system outputs 52
3.26 Effects of density and viscosity on system flow rate 53
4.1 Double-acting cylinder 59
4.2 Shuttle valve 60
4.3 Electrohydraulic actuator 60

Chapter 1

Introduction

1.1 Ankle-Foot Orthoses

Many technologies are being developed to assist the human body. These devices can help paralyzed people walk or recover from a stroke more quickly. Some devices are easily worn and portable, and others are stationary and immovable. An example of such a device that is worn on the body and provides assistance in movement is an ankle-foot orthosis (AFO). This device can be worn around the foot and ankle to provide supplemental assistance to a weak or impaired ankle or to augment the power at the joint. This assistance allows long term activities without fatigue.

Hydraulic technologies (pressurized fluid routed through conduits to allow actuation) are high force and low velocity applications. They can take the power of a motor which spins fast with low torque and transmit it with low velocity and high force. These characteristics match well to human joints making hydraulics a suitable source of power for an AFO.

In this chapter, the need for an ankle foot orthosis will be discussed. This will involve looking at how the ankle functions and can become impaired, at existing solutions to ankle impairments, and at the proposed solution of a hydraulic powered system. The results of this work are a design method for examining the requirements of the hydraulic powered system and a model for exploring variations and efficiencies of the system.

1.1.1 Ankle Function and Impairment

The ankle joint plays an important role in movement and walking. Walking consists of a series of events that are termed the gait cycle, illustrated in Fig. 1.1. The gait cycle consists of two parts, stance phase and swing phase. During stance phase, the specified limb is supporting the body weight. Stance phase is 62% of the cycle. During swing phase the opposite limb supports the body weight and the specified limb is clearing the ground and moving forward. 38% of the cycle consists of swing phase [1].

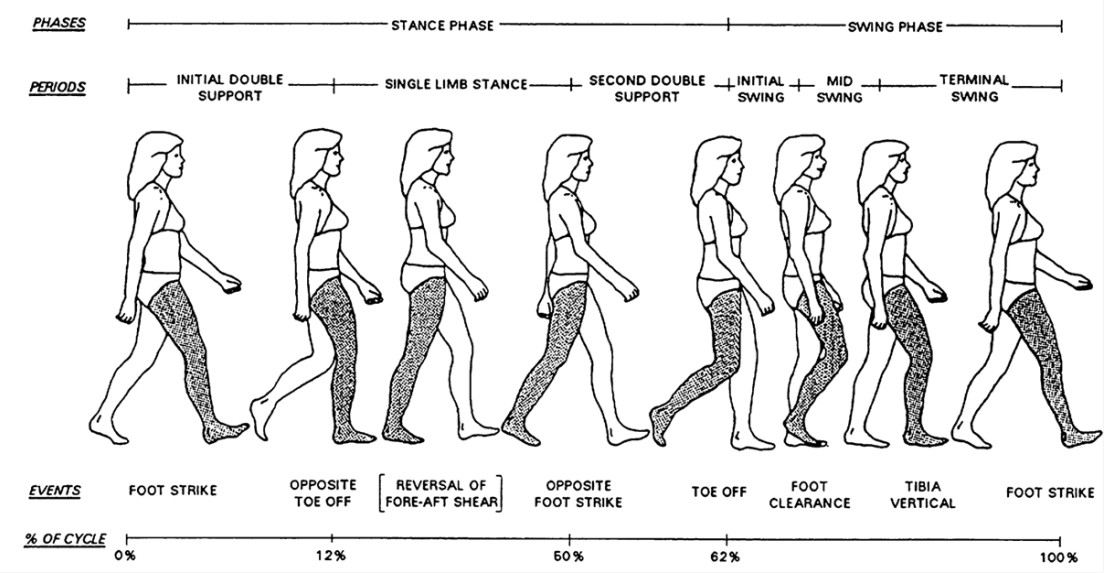

Figure 1.1: *The gait cycle is the time between successive foot contacts of the same limb. Image from [1].*

Examining the ankle more closely, it goes through two motions in the sagittal plane during the gait cycle. Plantarflexion, an increase in ankle angle, is used to achieve the push off force necessary for forward propulsion. Dorsiflexion, a decrease in ankle angle, is used to clear the ground during swing phase. The ankle motions can be described by looking at the torque or moment about the ankle joint and the angular velocity of the ankle joint during walking. The moment and angular velocity are the biomechanics of the joint. The ankle biomechanics taken from a normal, healthy individual (56.7kg) during level walking and showing ankle moment, angular velocity, and power are shown in Fig. 1.2. The ankle has a peak torque during push-off from stance to swing phase of

89 Nm and a peak power of 250 Watts [2].

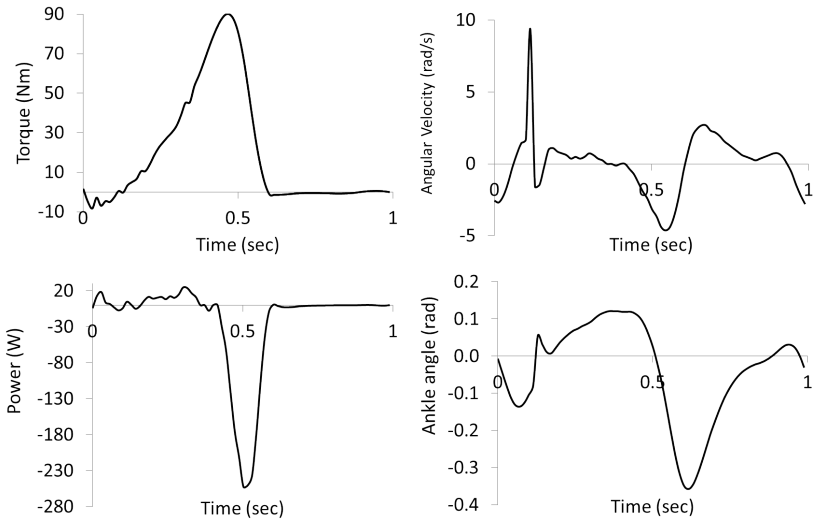

Figure 1.2: *Gait dynamics at the ankle measured in the saggital plane. Clockwise from the upper left, ankle torque, angular velocity, ankle angle, and power [2].*

The ankle functions under conditions other than level walking. Reiner [3] examined stair ascent and descent and observed that the ankle did not undergo large changes in power and torque whereas the knee and hip power patterns differed greatly from level walking. For jumping, Fukashiro [4] examined three jumps, squat jumps, countermovement jumps, and hops. Of the three movements, the ankle torques and powers were most changed from normal walking by the hopping motion.

Several pathologies and injuries can affect ankle function leading to impairment of gait. These pathologies most often result in ankle weakness and include trauma, incomplete spinal cord injury, brain injury, stroke, multiple sclerosis, muscular dystrophy, and cerebral palsy [5]. Muscle weakness can affect dorsiflexion muscles and plantarflexion muscles. Dorsiflexion weakness affects the ability of the toes to clear the ground and causes an altered gait where the leg must be flexed more at the hip and knee to allow clearance of the toes. This gait pattern is called foot drop. Plantarflexion weakness affects the stance phase of the gait cycle because the necessary torque for forward propulsion is not developed [6], resulting in reduced walking speeds.

An orthosis is a device that supports or corrects the functions of a limb and is intended to mechanically compensate for pathological conditions. An ankle foot orthosis

(AFO) is a device worn to lessen the impact of ankle impairments and weaknesses.Ankle-foot orthoses are the most commonly-used orthoses, making up about 26% of all orthoses provided in the United States [7]. An AFO surrounds the ankle and part of the foot and are often molded to each individual to allow the best fit. Clinically-available devices are a passive brace with some mechanical joint containing a spring or damper for motion control. Beyond clinically prescribed brace-type AFOs, research is exploring active or powered AFOs. An active orthosis is intended to assist persons with gait impairments through a means of augmenting the power at a joint [8]. An active orthosis has the potential of actively controlling the joints of the device. This requires an onboard or tethered power source, actuators for movement, sensors and a computer for controlling the force application. By allowing control of the joint and offering assistance in walking, these powered orthoses can operate as a daily walking assistance or a rehabilitation therapy device.

1.1.2 Passive AFOs

The most clinically prescribed AFOs are those that are static and only brace the ankle to avoid foot drop as seen in Fig. 1.3. These devices are lightweight, customizable, compact, and inexpensive. They are constructed of lightweight polypropylene-based plastic with one section molded to the shape of the wearer's calf and the other section to the foot. They can be articulated or nonarticulated at the joint. Articulated hinge joints are used to limit motion and optional springs resist or assist movement. Clinical AFOs brace the foot and keep it from dropping during swing, but also prevent it from flexing during plantarflexion. A review of passive AFOs is available in Shorter et al [9]. Due to the nature of the impairments and the requirements of the ankle during the gait cycle, a powered orthosis would better meet the needs of the user.

1.1.3 Active AFOs

There are several powered orthotics in the research phase. To understand how power is applied at lower limb joints, existing AFOs were studied along with other lower limb orthotics, exoskeletons, and prosthetic ankles. Dollar and Herr reviewed work in lower extremity exoskeletons and active orthoses in 2007 [8] and Shorter reviewed AFO

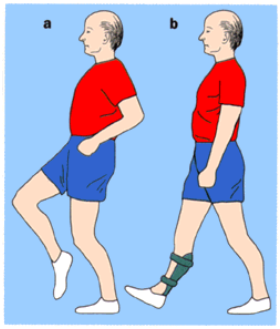

Figure 1.3: *Drop foot corrected by use of AFO. a. Uncorrected drop foot causes altered gait to compensate b. Corrected drop foot with an AFO. Image from [10]*

technologies and challenges in 2011 [9]. A summary of these and other literature resulted in Tables 1.1 for AFO and lower limb devices and 1.2, for exoskeletons and powered prosthetic devices.

In the orthosis category are devices that are meant for rehabilitation therapy and others for daily wear. Most are tethered to power sources or in the case of the CIRRIS AFO to a hydraulic master cylinder. Because many are research devices for gait measurement, gait perturbation, or rehabilitation, a tether is not prohibitive. The CIRRIS AFO [12], Arizona Robotic Gait Trainer [13], and Michigan AFO [19] are all fluid powered devices intended for such tethered use. Their capabilities allow them to be used for repetitive task therapy and strength building rehabilitation. The MIT AnkleBOT is actuated by two DC-motor-powered linear actuators for the same purpose of rehabilitation but also for purposes of measuring ankle joint properties [11]. The BIONic Walkaide and NESS L300 use functional electrical stimulation (FES) to directly stimulate a user's muscle to create force that powers the actuation [14, 15]. This can increase fatigue resistance and strengthen muscles however the patient population is limited. The MIT Active AFO and the Robotic Tendon from Arizona use different versions of series elastic actuators (SEA), where a motor-screw-spring arrangement allows manipulation of the compliance and elasticity of the orthosis [18, 16]. The stiffness and velocity of the SEA actuators developed at MIT by Pratt and Williiamson can be controlled for different walking speeds [17]. These devices are currently being configured to be untethered from their controllers and power sources.

The other devices listed in the table involve the ankle joint in some way and were

	Device	Functionality	Tethered	Mode of Operation	Ankle	Citation
AFO Devices	MIT AnkleBOT	Two DC-motor powered linear actuators	Tethered	Electromechanical		[11]
	CIRRIS AFO	Water-filled hydraulic master cylinders and run by electric motor and driving a slave cylinder	Tethered	Hydraulic		[12]
	Arizona State Robtic Gait Trainer	Pneumatic Spring Over Muscle actuators with McKibbon style pnuematic muscle	Tethered	Pneumatic		[13]
	BIONic WalkAide	FES, commerically available	Untethered	Electrical		[14]
	NESS L300	FES, commerically available	Untethered	Electrical		[15]
	Arizona State Robotic Tendon AFO	Robotic tendon (modified series elastic actuator)	Tethered	Electromechanical		[16]
	MIT Active AFO	Series elastic actuator	Tethered	Electromechanical		[17, 18]
	Michigan AFO	McKibben style articial pneumatic muscles, controlled by EMG signals	Tethered	Pneumatic		[19, 20, 21]
	UIUC PPAFO	Pneumatic rotary actuator	Untethered	Pneumatic		[22]
Lower Limb Devices	Hydraulic stance control knee mechanism (SCKM)	Locks knee during stance with hydraulic cylinder and solenoid valve	Untethered	Hydraulic	Constrained	[23]
	Lower limb orthosis with bi-lateral-servo actuator	Master-slave cylinder, with slave having two rods	Tethered	Hydraulic	Slave cylinder	[24]
	Hybrid neuro-orthosis	FES controlled joints	Untethered	Electrical	FES implants	[25, 26, 27]
	Ankle and knee pertubator	Bowden wires connect joint to motor and double pneumatic cylinder	Tethered	Mechanical	Mechanical joint	[28]

Table 1.1: *AFO and lower limb technology describing functionality of device, whether or not it's tethered to a power source, mode of operation, and ankle actuation mechanisms.*

	Device	Functionality	Tethered	Mode of Operation	Ankle	Citation
Exoskeletons	Esko	Four Servomotors	Untethered	Electromechanical	Static	
	ReWalk	Servomotos	Untethered	Electromechanical	Static	
	Berkley-BLEEX	Electric actuation with hydraulic transmission	Untethered	Electrical	Electric actuator	[29]
	MIT exoskeleton	Quasi-passive design for controlled release of stored energy at joints	Untethered	Passive stored energy	Springs	[30]
	Hybrid assistive leg (HAL)	Augment joint torques with DC motor directly on joints	Untethered	Electromechanical	Static	[31]
	Nurse assisting exoskeleton	Direct-drive pneumatic rotary actuators for knees and hips	Unknown	Pneumatic	Static	[32]
Powered Prosthesis	Transfemoral prothesis	Springs and DC motors in series	Untethered	Electromechanical		[33]
	MIT powered ankle-foot prothesis	Combination of DC motor, transmission elements, series elastic actuator, and parallel spring	Untethered	Electromechanical		[34]
	SPARKy 3	2 sets of DC motor, roller screws, springs to allow extension and flexion and inversion and eversion	Untethered	Mechanical		[35]

Table 1.2: *Exoskeleton and prosthetic technology describing functionality of device, whether or not it's tethered to a power source, mode of operation, and ankle actuation mechanisms.*

included for their power mechanisms. The lower limb devices are a range of laboratory devices with one being a knee stance control mechanism developed at Case Western that locks the ankle in order to study the knee [23]. Saito and his collegues at Tokyo Denki University have developed an knee-ankle-foot orthosis that uses a system of master and slave cylinders, though the power source and actuation scheme are unclear [24]. The neuroprothesis by Kobetic at Case Western controls all joints with implanted electrical stimulation electrodes [25]. Andersen and Sinkjar have created an ankle-knee perturbator using a mechanical design with Bowden wires and a clutch system to introduce a disturbance into the gait and study gait compensatory patterns after a perturbation [28]. These designs represent four ankle mechanisms; static brace, master-slave cylinders, electrical stimulation, and a mechanical clutch system. The static brace and clutch system only serve to lock the ankle. The master-slave cylinder actuator has an unclear power output and electrical stimulation causes rapid muscle fatigue that makes it a non-ideal power source [25].

Exoskeletons are intended to augment the power of limbs to aid in movement and are worn like artificial limbs. The lower limb exoskeletons concentrate their power and actuation on the knee and hip joints while leaving the ankle joint either constrained or subject to the passive energy storage of a spring [32]. Two commercially available exoskeletons exist. Both the Esko Bionics (`www.eksobionics.com`) and the ReWalk (`www.argomedtec.com`) use servomotors at the hip and knee joints while leaving the ankle as a passive pivot joint. The Berkley lower extremity exoskeleton (BLEEX) controls power usage by not actively powering the ankle joint, but allowing it to actuate with natural movement [29]. Because this exoskeleton is intended to supplement power, it is assumed that the ankle can function under its own power. The BLEEX powers the knee and hip joints using hydraulic actuators controlled by servo-valves that achieve very favorable joint torques. Similar to the BLEEX, the MIT exoskeleton is designed to transfer a load in a backpack directly to the ground. The MIT design is passive actuation with series elastic actuators that control spring damping at hip and an energy storing spring at the ankle [30]. Kawamoto et al developed a Hybrid Assistive Leg (HAL) which provides assistive power to the hip and knee joints via DC servo motor actuators in combination with harmonic drive gears powered by a backpack mounted battery [31]. The HAL design has braced ankles to reduce complexity of control and

power. The Nurse Assisting Suit by Yamamoto et al consists of shoulders, arm, waist and legs that are fitted on the body [32]. The elbow, hip, and knee joints are actuated by pneumatic rotary actuators utilizing balloon-like pressure cuffs. The output torque of these joint actuators were half of what was required by the biomechanics of the joint. The Nurse Assisting Suit provides no ankle power. The exoskeleton designs do not provide power to the ankle and their power mechanisms are not ideal, either large and heavy or weak and passive.

There are many powered ankle prosthetics but only a few are shown in Table 1.2. The field of prosthetics is too vast to include a complete study of all mechanisms. They include a variety of ways of powering the gait but because they are replacing the ankle itself, they have the freedom of more space and not needing to work with the natural joint [33, 34, 35].

Current clinical AFOs are light and compact. They can improve gait at particular gait cycle points but can impede later points in the gait cycle. They do not provide assistive torque at the ankle. Articulated devices with springs can be beneficial during certain gait patterns, but cannot be controlled to adapt to different conditions. Powered AFOs provide assistive torque at the ankle during gait. To provide this torque many of the AFOs and lower limb orthotics studied here used large and bulky actuators that are not easily concealed under a pant leg. For their size, many of the AFOs and lower limb orthotics were not capable of the full range of power needed throughout the gait cycle. The exoskeletons designs chose to limit power to the ankle altogether. The size and power requirements of these designs require systems that are tethered to power sources and controllers. Thus there is a need for devices that provide full ankle power without being bulky and heavy.

1.2 The Hydraulic-powered Ankle-Foot Orthosis

Design requirements for a powered ankle-foot orthosis must account for gait dynamics as well as the comfort of the user. Requirements include: light, compact, noise-free, portable/untethered, and the ability to provide sufficient power, torque, and velocity output. Light means that the device does not increase the energy expenditure of the user or inhibit gait. Compact implies an unobtrusive device that is space efficient. These

requirements limit the power of the device because it cannot have a large cumbersome power source or heavy transmission. Current battery technology is not advanced enough to allow a compact power source to output high power for several hours. If the ankle device is purely a rehabilitation device, then it is permissible to be tethered to a desktop power source or computer to allow for more complex control and higher power output.

Fluid powered systems have the potential to improve orthotics. Many of the AFO devices in Tables 1.1 and 1.2 use fluid power in some capacity. Shorter has written a review of powered-orthotic devices [9] and explains well why this technology would be successful in orthotics. Human motion is powered by high torques at relatively low velocities whereas electric motors operate in opposition to this in the low torque and high velocity range and thus a transmission element is needed. These transmission elements can be heavy and must be co-located with the joint axis to provide the output necessary thus creating a bulky and heavy system. Fluid power is advantageous for many reasons including high force to weight ratio and force to volume of the actuator, the ability to actuate without a gear or ball screw at the joint, and the ability to transport the pressurized fluid through flexible tubing in ways the shaft of a motor cannot. Being able to configure the system by routing fluid allows the system to be compact and efficiently fill a space.

Fluid power can be done with pressurized fluids (hydraulics) or pressurized gases (pneumatics). For the AFO, hydraulics have significantly less losses to compressibility, transmit higher forces, and create less heat compared to pneumatic systems. The air in pneumatic systems is compressible causing spongy losses and extra heat from the compression process as well the inability to transfer high amounts of force. There are challenges associated with hydraulics mainly due to decreasing the size to accommodate orthotic applications [36]. Traditional applications use the high forces of hydraulics to lift heavy loads resulting in large, heavy components. If hydraulics can be designed to be efficient at small scales, then they accomplish the requirements of being lightweight and compact. Their high force transfer ability would allow hydraulics to be used for dorsiflexion and plantarflexion assistance both in a daily use and rehabilitation setting.

1.2.1 Power Transmission Design

In choosing a hydraulic solution to the powered ankle-foot orthosis, there are several possible realizations of power transmissions. There must be a way of creating high pressure fluid, a way of transporting and controlling it, and a way of converting it to a joint actuation. Hydraulic pumps are used to create high pressure fluid, the same way air compressors create pressurized air for pneumatics applications. Tubing and hoses can be used as conduits to route the pressurized fluid from the pump to the joint, they are able to bend and flex to allow different system configurations. The actuation can be a linear actuator like a hydraulic cylinder or a rotary actuator. Depending on how the system is controlled, valves can be used to direct fluid flow and control the motion of the actuator.

For this study, one hydraulic power transmission configuration was chosen. The power transmission path is shown in Fig. 1.4. The energy source is a battery. This provides voltage to a DC-motor which spins a pump shaft. The pressurized fluid created by the pump is routed through pipe to a linear actuator. This actuator is a double-acting hydraulic cylinder whose motion acts on a moment arm about the ankle joint creating a torque. Each side of the double-acting cylinder is connected to one of the pumps outlets. The system is controlled with the bidirectional pump to pressurize either side of the cylinder and cause actuation.

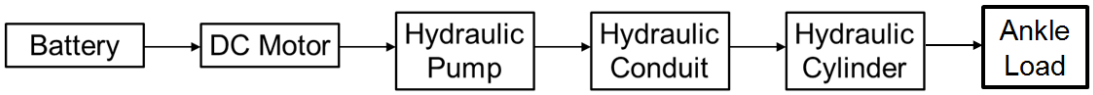

Figure 1.4: *Power transmission elements in the HAFO design. The battery provides electrical energy to the motor. The motor provides rotational power to the pump. The pump transforms this to fluid power in terms of pressure and flow through the conduits. The hydraulic cylinder transforms this into linear force and velocity that is applied at the moment arm of the ankle to create ankle torque and velocity.*

This design was chosen because of its linearity and flexibility. The output of each element is related to the input of the next by a component parameter and efficiency. Altering a parameter of the motor changes its output, affecting the input to the pump, and therefore the power to the whole system. The “across variables” and “through

variables" of each element in the power transmission relate to the ankle dynamics because torque and angular velocity are the two key factors that the orthosis must control. This linearity allows an understanding of how one parameter change affects the whole system. The design is flexible because different components can be packaged together and hydraulic power routed between them.

The power transmission was analyzed with a model (using Matlab©) to allow for further study of its components and their interactions. The model was validated on a hardware prototype.

1.2.2 Research Objective

This thesis had two objectives. The first was to create design requirements for this hydraulic power transmission for an AFO by working inversely from the ankle dynamics (torque and velocity) back through the components. The second was to create and validate a model for the power transmission that can be used to test future iterations. The outcomes of these activities were design requirements for sizing the geometric properties of the components and an understanding of system behavior and efficiency.

Chapter 2

Methods

2.1 Mapping Transmission Requirements

The goal was to provide a method that works inversely from known ankle kinetics to inputs and outputs of each component of the HAFO power transmission. The transmission design from Section 1.2.1 is shown in Fig. 2.1 where listed along with the components are their energetic variables. Each component has across variables and through variables for output. Fig. 2.2 illustrates the interaction of each component in relation to the next, along with the physical parameters that describe this relationship. The system parameters are defined in Table 2.1.

The objective of the method was to 1) determine the power transmission needed in each component and 2) vary the physical parameters for comparison of system configurations using simplified models of each component.

The known ankle kinetics were the torque and angular velocity needed for gait. These were obtained from literature records of gait analysis, for example the plots from Fig. 1.2. The hydraulic cylinder supplies linear force and velocity about the pivot point of the ankle that translates into the necessary ankle torque and angular velocity. The force F and linear velocity v from the ankle torque T_1 and angular velocity ω_1 are

$$F = \frac{T_1}{r} \tag{2.1}$$

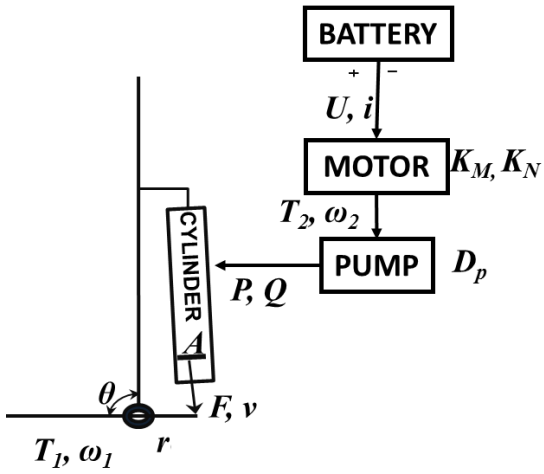

Figure 2.1: *Across and through variable elements between each component of the prototype and how the moment arm acts at the ankle to provide torque and angular velocity.*

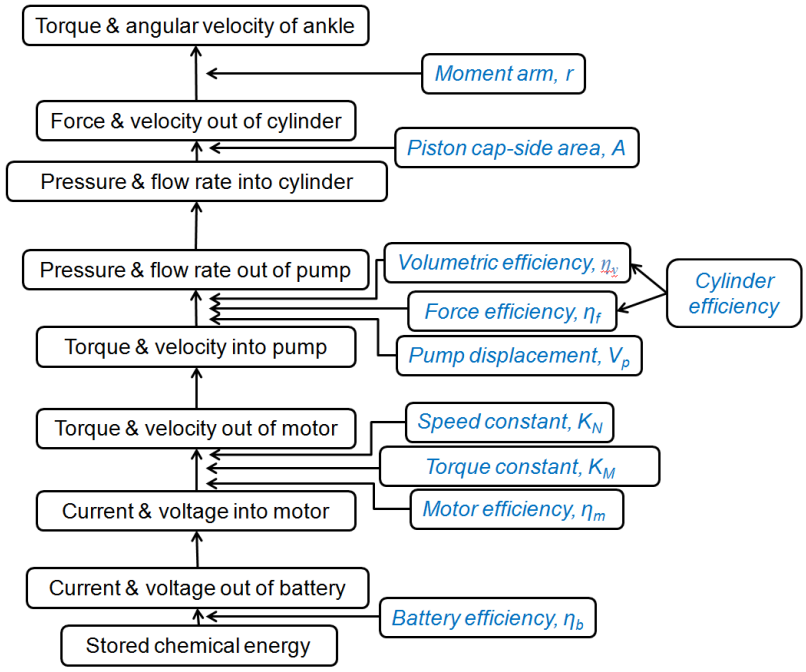

Figure 2.2: *The interactions of each component in the power transmission and which physical parameters effect these interactions.*

Symbol	Description	Unit
T_1	Ankle torque	Nm
θ	Ankle angle	deg
ω_1	Ankle angular velocity	rad/sec
r	Moment arm at ankle	m
F	Piston force	N
v	Piston velocity	m/s
A	Piston cap-side area	m^2
P	Piston cap-side pressure	Pa
Q	Piston cap-side flowrate	m^3/sec
η_{f1}	Cylinder force efficiency	–
η_{v1}	Cylinder volumetric efficiency	–
P	Pump pressure	Pa
Q	Pump flowrate	m^3/sec
D_p	Pump displacement	m^3/rad
η_{f2}	Pump force efficiency	–
η_{v2}	Pump volumetric efficiency	–
T_2	Pump torque	Nm
ω_2	Pump velocity	rpm
K_M	Motor torque constant	mNm/A
K_N	Motor speed constant	rpm/V
T_2	Motor torque	Nm
ω_2	Motor velocity	rad/sec
η_m	Motor torque efficiency	–
i	Motor current	A
U	Motor voltage	V

Table 2.1: *System parameters used in the inverse requirements method.*

and

$$v = r * \omega_1 \tag{2.2}$$

where r is the moment arm at the ankle and θ is the angle of the ankle. Power losses in the moment arm were assumed to be negligible.

The force and velocity of the cylinder piston result from the pressure and flow rate of the fluid inside the cylinder provided by the pump. The pressure P and flow rate Q from force and linear velocity needed at the piston is

$$P = \frac{F}{A * \eta_{f1}} \tag{2.3}$$

$$Q = \frac{v * A}{\eta_{v1}} \tag{2.4}$$

where the volumetric and force efficiencies, η_{v1} and η_{f1}, of the cylinder are assumed to be constant, and A is the area of the piston cap that the pressure acts on.

The pressure and flow rate of the pump were created by the torque and shaft velocity of the motor on the pump. The torque T_2 and velocity ω_2 are calculated using the pump displacement D_p and pump efficiencies, η_{v2} and η_{f2}

$$T_2 = \frac{PD_p}{2\pi\eta_{f2}} \tag{2.5}$$

$$\omega_2 = \frac{Q}{D_p\eta_{v2}} \tag{2.6}$$

The current i and voltage U needed by the motor in order to supply the needed torque and velocity are calculated using the motor speed constant K_N, motor torque constant K_M, and motor efficiency η_m

$$i = \frac{T_2}{K_M\eta_m} \tag{2.7}$$

$$U = \frac{30\omega_2}{\pi K_N} \tag{2.8}$$

From these equations plots can be generated for each component: the across variable output of the component versus gait cycle time, the through variable output of the component versus gait cycle time, the across variable versus the through variable output, and power of the component versus gait cycle time. The power for the component was calculated by multiplying the across variable term by the through variable term. Viewing the curve over the whole gait cycle allows a view of what is required of each component throughout the gait cycle. A Matlab©GUI was created to run the calculations (Appendix A).

A comparison between parameters was made by setting all parameters and then altering only one parameter to see the effect on the transmission. In the case of the prototype, the parameters are determined by combinations of the component dimensions and their particular output characteristics. The limited selection of available components narrows the possible combinations of components, but when components are custom fabricated this method can be used to optimize the requirements of each component.

2.2 Model

The HAFO hydraulic circuit model consisted of a DC brushed motor, a fixed displacement bidirectional piston pump, pipelines, check valves, and double-acting hydraulic cylinder as shown in Fig. 2.3. This system is controlled by running the bidirectional pump in either direction to control flow to the desired end of the cylinder. A high-efficiency controllable motor will be added between the battery and the motor. Because the system acts on a fixed moment arm with a 30 degree range of motion at the ankle, the model is simplified to output only at the force acting on the piston and the velocity of the piston. Fluid properties were included in the model.

Two approaches were taken for the model. The first was a set of dynamic equations and the second was an object-oriented model. The dynamic equations were used as basic affirmation of model behavior. The object-oriented model was a component-wise

description of the system.

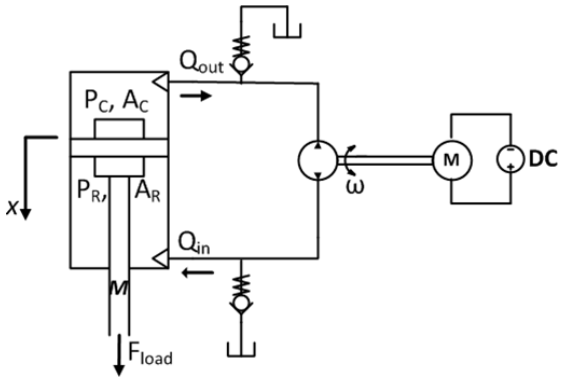

Figure 2.3: *The HAFO system included a dc-motor, fixed displacement piston pump, valves, pipelines, double-acting cylinder.*

2.2.1 Dynamics-oriented model

The dynamic equations of the piston system are expressed by the following relationship [37]

$$M\ddot{x} = P_R A_R - P_C A_C - F_{load} - D\dot{x} \tag{2.9}$$

where M is the mass of the piston and rod, x is the position of the piston, P_R and P_C are the pressures in the rod side and cap-side of the cylinder respectively, A_R and A_C are the areas of rod-side and cap-side of the piston, F_{load} is the rod force, and D is the damping in the piston.

The change of rod-side pressure during piston retraction is described by (2.10). Retraction was studied because it is the direction causing plantarflexion in the AFO and needs to provide the highest force.

$$\dot{P_R} = \frac{E_{effective}}{V_R}(Q_R - A_R\dot{x}) \tag{2.10}$$

where $\dot{P_R}$ is the change in rod-side pressure, $E_{effective}$ is the effective bulk modulus of the fluid, V_R is the volume of the cylinder on the rod-side, Q_R is the flow rate into the rod-side, and x is the postion of the cylinder cap. Here the difference between flow into

the cylinder and the velocity of the piston multiplied by the area of the rod-side describe the flow used to compress of the fluid due to its bulk modulus, $E_{effective}$. When divided by the volume of the liquid on the rod-side, this described the change in pressure in the rod-side of the cylinder. Integrating gives the pressure in the chamber [37].

2.2.2 Object-oriented model

The object-oriented model looked at each component in Fig. 2.3 and used a model of each component to solve the piston force and rod-side pressure. The components will be described here starting from the speed input to the motor and working through each component's fundamental equations. Variables are listed in Table 2.2. Each component has an across variable and through variable equation.

The DC-brushed motor is modeled by the following equations, one describing the electrical side [38]

$$V_{in} = K_b\omega + iR + L\frac{di}{dt} \tag{2.11}$$

where V_{in} is the voltage into the motor, i is the current, K_b is the motor voltage constant, ω is the shaft speed, R is resistance, and L the inductance. The other motor equation describes the mechanical side [38]

$$T_{out} = K_t i - J\frac{d\omega}{dt} - T_{friction} - T_{load} \tag{2.12}$$

where T_{out} is the torque output, K_t is the motor torque constant, J is the moment of inertia of the rotor, and $T_{friction}$ and T_{load} are the torque to friction and the torque due to the load, respectively. From these equations the motor current draw and torque output of the motor can be found. The model controlled this motor with a speed-control loop by measuring output shaft speed of the motor and adjusting motor voltage to maintain desired output speed. The control loop was a PID controller with a proportional constant of 0.09 and an integral constant of 0.75. This mimiced the controller in the prototype.

The pump is described by two equations, for flow rate and pressure. Flow rate is

Symbol	Description	Unit
V_{in}	Motor voltage	V
ω	Shaft speed	rpm
K_b	Motor voltage constant	V/rpm
i	Motor current	A
R	Motor resistance	Ω
L	Motor inductance	mH
T_{out}	Motor output torque	Nm
K_t	Motor torque constant	Nm/A
J	Rotor moment of inertia	gcm^2
$T_{friction}$	Torque to friction	Nm
T_{load}	Torque to load	Nm
Q_{pump}	Pump output flow rate	m^3/sec
D_p	Pump displacement	m^3/rad
k_{leak}	Leakage coeffecient	–
k_{HP}	Hagen-Poiseuille coeffecient	–
ν	Viscosity	cSt
ρ	Density	kg/m^3
η_{vol}	Pump volumetric efficiency	–
ω_{nom}	Nominal pump speed	rpm
p_{nom}	Nominal pump pressure	psi
$P_{discharge}$	Pump output pressure	psi
η_{mech}	Pump mechanical efficiency	–
η_{total}	Pump total efficiency	–
ΔP	Pressure drop in conduit	psi
f	Conduit friction coefficient	–
L	Conduit length	m
D	Conduit inner diamter	m
w	Conduit flow velocity	m/s
F	Rod force	N
A	Area of cylinder	m^2
P	Pressure in cylinder	psi
v_{piston}	Piston velocity	m/s
$Q_{leakage}$	Pump leakage flow	m^3/sec
V_o	System dead volume	m^3
$E_{effective}$	Effective bulk modulus	Pa
Q_{comp}	Flow to compress fluid	m^3/sec
C_d	Orifice flow discharge coeffecient	–
E_l	Liquid bulk modulus	Pa
α	Relative gas content of liquid	–
p_a	Atmospheric pressure	Pa
n	Gas specific heat ratio	–

Table 2.2: *Model parameters.*

calculated by [39]

$$Q_{pump} = D_p\omega - k_{leak}p \tag{2.13}$$

where Q is flow rate out of the pump, based on pump displacement D_p, and shaft speed ω, and a leakage coefficient. The leakage coefficient is found by [39]

$$k_{leak} = \frac{k_{HP}}{\nu\rho} \tag{2.14}$$

k_{HP} is the Hagen-Poiseuille coefficient defined as follows [39]

$$k_{HP} = \frac{D_p\omega_{nom}(1-\eta_{vol})\nu_{nom}\rho}{p_{nom}} \tag{2.15}$$

where D_p is pump displacement, ω_{nom} is the nominal speed of the pump at the nominal pressure p_{nom}, η_{vol} is the volumetric efficiency at the nominal speed and pressure, and the fluid properties are defined by nominal kinematic viscosity ν_{nom} and density ρ.

Pressure $P_{discharge}$ created by the pump is related to the torque T of the motor on the shaft of the pump

$$T_{out} = \frac{D_p P_{discharge}}{\eta_{mech}} \tag{2.16}$$

where D_p is the pump displacement and the η_{mech} is the mechanical efficiency of the pump. The mechanical efficiency is found by η_{ltotal}/η_{vol}.

From the motor's shaft speed and torque, the velocity and force of the system are translated to flow and pressure in the pump and then are passed through pipelines to the cylinder. The pressure drop in the conduit, ΔP is described by [40]

$$\Delta P = \frac{0.5 f w^2 \rho L}{6895 D} \tag{2.17}$$

where f is the friction coefficient (calculated using Reynolds number, which is dependent on density, hose ID, and dynamic viscosity), w is the flow velocity, ρ is the fluid density,L is the length of pipe, and D is the inner diameter. This model is for flow through circular cross-sections with an assumption of steady-state, fully developed flow.

The rod force is

$$F = A_R P_R - A_C P_C \tag{2.18}$$

where F is the rod force acting on the load, A_C and A_R are the areas of the cap-side and rod-side of the cylinder, and P_C and P_R are the pressures at each end of the cylinder. This model does not account for piston and rod-seal friction and assumes a massless rod and piston.

Pump output flow rate is described by the following

$$Q_{pump} = Q_{leakage} + Q_{comp} + A_R v_{piston} \tag{2.19}$$

where A_R is the area of the rod-side cylinder, V_{piston} is piston velocity, $Q_{leakage}$ is leakage flow in the cylinder, and Q_{comp} is flow to fluid compression. Fluid flow used to compress the fluid, Q_{comp}, is defined by [39],

$$Q_{comp} = \frac{V_o + A(x_o + x * or)}{E_{effective}} \cdot \frac{dp}{dt} \tag{2.20}$$

where V_o is the dead volume (volume in cylinder end when dead-stopped plus internal system volume of hoses and pump), A is cross-sectional area of the specified cylinder end, x is the position of the piston, x_o the original postion of the cylinder, *or* the sign of the change in position, p is the differential pressure, and $E_{effective}$ is the effective bulk modulus.

Cylinder leakage was modeled as an orifice in parallel with the perfectly efficient cylinder, where flow through the leakage orifice, $Q_{leakage}$ was modeled by

$$Q_{leakage} = C_d A \sqrt{\frac{2}{\rho} p} \tag{2.21}$$

where C_d is the flow discharge coefficient of the orifice, A is the area of the orifice, ρ the fluid density, and p is the pressure differential across the cylinder equal to $P_R - P_C$.

2.2.3 Fluid properties

The three fluid properties used in the model were kinematic viscosity ν, density ρ, and effective bulk modulus $E_{effective}$.

The effective bulk modulus was [41]

$$E_{effective} = E_l \frac{1 + \alpha(\frac{p_a}{p_a+p})^{1/n}}{1 + \alpha \frac{p_a^{1/n}}{n \cdot (p_a+p)^{\frac{n+1}{n}}} E_l} \tag{2.22}$$

where E_l is the liquids defined bulk modulus, α is the relative gas content of the liquid, p_a is the atmospheric pressure, p is the gauge pressure of the liquid in the chamber, and n is the gas-specific heat ratio of the liquid. The working fluid used in the prototype and in the model was mineral oil with a bulk modulus of 1.8e9 Pa, density of 870 kg/m^3, and a viscosity of 40 cSt.

2.2.4 Implementation

The model was realized in Matlab's Simulink platform, SimHydraulics. The equations for each component were packaged in a SimHydraulics block that allowed for assembly of the model by connecting the correct component blocks and providing the desired input values for shaft speed and piston load force. Appendix B shows the simulation diagram of the model.

To validate that the model could represent an actual system, the model parameters were tuned to match the parameters of the HAFO prototype. The hardware prototype was first tested to gather parameters for the model. The micro axial piston pump and DC-brushless motor were tested individually to understand their efficiencies. The system as a whole was then tested and compared to the model in a series of simulations.

2.2.5 Model objectives

To make design recommendations the model had to be capable of the following objectives:

- Simulate behavior as described by Equations (2.9) and (2.10).

- Demonstrate whether or not the transmission design can satisfy the necessary gait requirements.
- Demonstrate the effect of geometry on the efficiency of the components and the overall system efficiency.
- Demonstrate how fluid properties affect system performance.

The model was used to make recommendations for the capabilities of the system, the geometry of the components, and the working fluid choice.

2.3 Model Validation

A prototype of the power transmission design was implemented on an ankle-foot orthosis to act as a validation of the model.

The prototype was built using off-the-shelf components to reduce cost as well as demonstrate the need for further development of small hydraulic technology (Fig. 2.4). The double acting hydraulic cylinder was mounted on the rear of AFO and acts on a moment arm that applies the cylinder output force as torque at the ankle. Using flexible copper tubing, the pump and motor unit were mounted parallel to the cylinder providing a package that is wholly contained on the AFO shell. The motor controller and battery pack were placed in a small package carried on the user. A fluid power schematic shows the connections of the different components (Fig. 2.5).

The fluid power schematic was a modified Electro-Hydraulic Actuator (EHA) that uses a motor to power a reversible pump that actuates a hydraulic cylinder [42]. Commercially available EHAs have precautionary pressure relief valves, pilot-operated check valves (allow for load holding), and a series of pilot-operated relief valves (relieve the excess fluid). These EHAs are large and meant for forces much higher than the ankle requires so the extra valves are necessary. For the AFO application the check valves allow volume compensation without the bulk of many valves. The check valves act as pressure relief valves in the system.

The battery was a 23V (Thunder Power 2250mAh 22.2V 6 Cell Lithium Polymer, TP-2250-6SP30) powering a Maxon DC-brushless flat motor (370426) connected to a Takako micro axial piston pump (THF-040, 0.4cc/rev displacement). The double acting

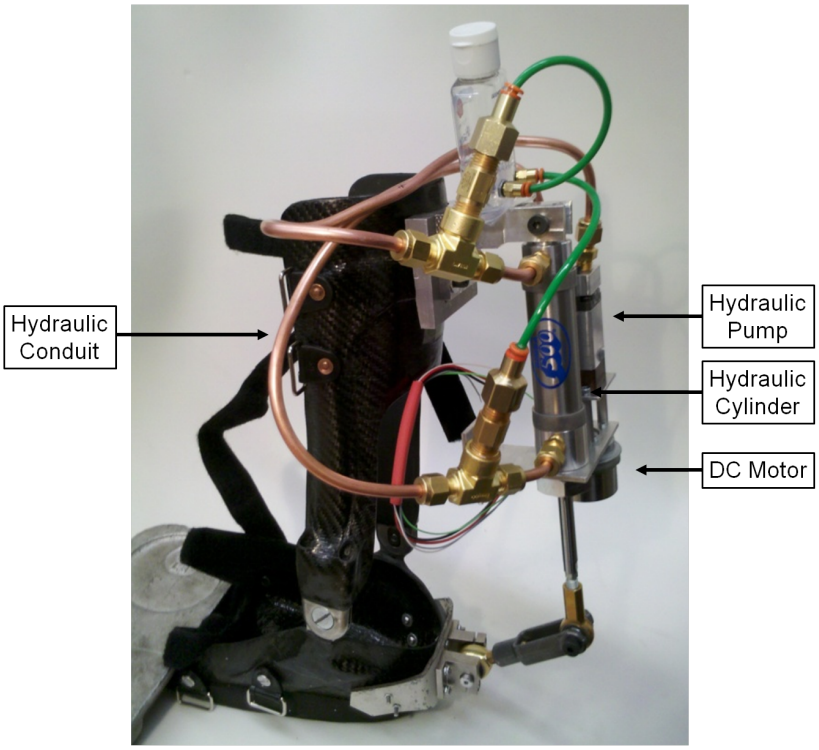

Figure 2.4: *The HAFO hardware prototype showing the main elements of the power transmission mounted on the AFO brace, motor and pump mounted parallel to the cylinder with the copper tubing connectring the pump to the cylinder and allowing attachment of the valves.*

cylinder was from Bimba (H-092-DUZ) and could operate up to 500 psi. The AFO shell was custom made. Check valves (Swagelok B-4CPA2-150 and B-4CP2-1) are needed to compensate for the volume differences in pumping from the cap-side of the cylinder to the rod-side of the cylinder.

To validate that the model could represent an actual system, the model parameters were tuned to match the parameters of the HAFO prototype. The hardware prototype was first tested to gather parameters for the model. The micro axial piston pump and DC-brushless motor were tested individually to understand their efficiencies. The system as a whole was then tested and compared to the model in a series of simulations.

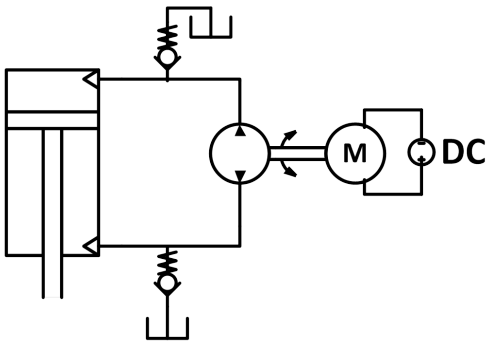

Figure 2.5: *A hydraulic circuit of the prototype showing the connections between the power transmission elements. The battery provides current and voltage to the motor. The motor provides torque and angular velocity to the pump, which creates a flow rate and pressure in the fluid that acts on the piston cap to move the piston. This results in force and linear velocity at the piston. Check valves are needed to compensate for the unequal fluid volumes.*

2.4 Parameter determination

The model was tuned based on prototype parameters. The model parameters determined experimentally included pump efficiency, motor torque-speed, and cylinder leakage orifice area. Other parameters were geometric and determined by the size of the components such as cylinder bore diameter, cylinder areas, and pipe dimensions. The remainder of the parameters needed for the model were set by data sheet values such as motor internal resistance and inertia, check valve cracking pressure, and fluid properties. Table 2.3 shows the parameters of the system.

2.4.1 Motor parameters

The motor's torque-speed curve was determined experimentally. The Maxon motor was tested on a dynamometer (Magtrol HD-710)[1] , Fig 2.6. The shaft speed was set to five values (900, 1400, 2000, 3000, and 4950 rpm), and at each speed setting the motor was run through four torque values (5, 10, 15, 20 in-oz) with a 2 second dwell time at each torque. The supply voltage was set at 24 volts, the nominal voltage from the data sheet. The speed response of the motor was recorded along with current draw to

[1] Tests were conducted Parker Hannafin Oildyne Division

Component	Variable	Symbol	Value	Unit
Fluid Properties	Bulk modulus	E	1.8e9	Pa
(Mineral Oil)	Density	ρ	870	kg/m^3
	Viscosity	ν	40	cSt
Cylinder Properties	Area of cap	A_c	0.000572	m^2
	Area of rod-side	A_R	0.000496	m^2
	Dead volume cap-side	V_0	100	mL
	Dead volume rod-side	V_0	100	mL
	Piston mass	M	0.06	kg
Pipe	Pipe ID	D	2.4	mm
	Pipe length	L	2	m
Pump	Displacement	D_p	0.4	cc/rev
Motor	Inertia	J	193	gcm^2
	Speed constant	K_N	600	rpm/V
	Internal resistance	Ω	0.567	Ohm
	Inductance	L	0.413	mH
Motor PID Controller	P constant	P	0.09	
	I constant	I	0.75	
Check valve	Cracking pressure	p	125	psi

Table 2.3: *Component parameters used for validation of the model based on the geometries of the hardware prototype, fluid properties, and data sheet values.*

calculate efficiency. Efficiency was calculated by

$$\eta_t = \frac{P_{out}}{P_{in}} = \frac{\omega T}{Vi} \tag{2.23}$$

where ω is the shaft speed, T is the output torque, V is voltage, and i is the current.

The Maxon motor is a combination motor and speed controller. The plots of the torque speed curve show motor behavior and were used in the model to set the constants in the PID speed controller that represented the motor speed controller. The PID controller had a proportional constant of 0.09 and an integral constant of 0.75.

2.4.2 Pump parameters

Pump parameters needed were the volumetric and force efficiency, therefore shaft speed and torque in and pressure and flow rate out were determined experimentally. The Takako axial piston pump was tested using a drive motor (Baldor motor M3158 and

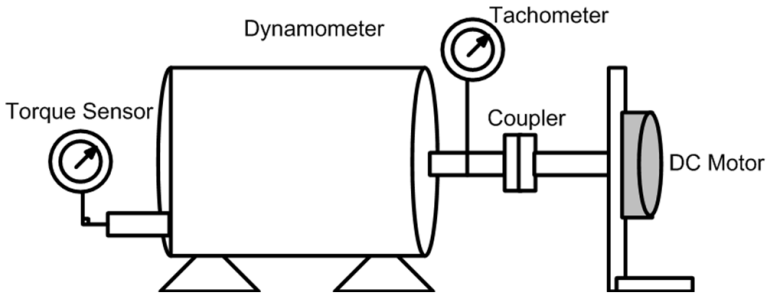

Figure 2.6: *The Maxon motor was tested with a dynamometer where shaft speed and torque were recorded.*

variable frequency drive R-ID15J203-ER) connected to a torque sensor (Lebow 1602-1K) to provide an input speed and measure shaft torque. The flow rate was measured with a flow transducer (AW Company CAPM-2 and JVM-20KL) while the pressure was set by a needle valve and measured using an inline pressure sensor (Ashcroft 25D1005PS02L5000-B1)[2] . Test stand illustrated in Fig 2.7.

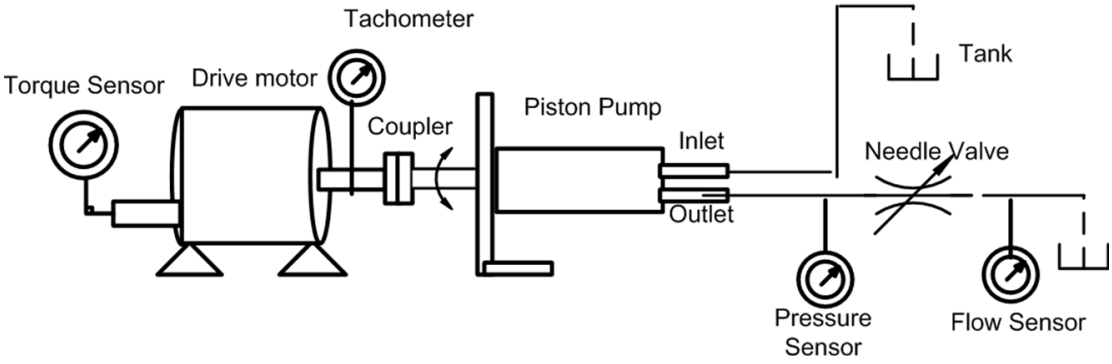

Figure 2.7: *The Takako axial piston pump was tested with a drive motor and needle valve where shaft speedand pressure were set while torque and flow rate were recorded.*

Five shaft speeds (459, 804, 1437, 2012 rpm) and five pressure values (100, 500, 1000, 1500, 2000 psi) were tested. At each set shaft speed, the flow rate was recorded after the needle valve was adjusted to set the system pressure of each of the test pressure points. At each pressure point, the motor shaft torque was recorded. Torque versus pressure was plotted at the five shaft speeds, and flow rate versus shaft speed was plotted at the

[2] Tests were conducted at Parker Hannafin Oildyne Division

five pressures. The force efficiency was found as the inverse slope of the torque versus pressure line divided by pump displacement (in (2.16)). The volumetric efficiency was found as the slope of the flow rate versus speed line divided by the pump displacement, from a simplified (2.13). The total pump efficiency found by dividing power out by power in and was plotted versus power output. To find a nominal value of total efficiency for the simulation, the volumetric efficiency at the desired operating pressure was multiplied by the mechanical efficiency. The power versus total efficiency curve was compared to the model output to see the behavior of the pump model compared to the actual pump.

2.4.3 Cylinder parameters

Leakage across the cylinder was not available via data sheet and therefore was determined experimentally. The model used an orifice in parallel with the cylinder to model this leakage, (2.21). The area of this orifice was needed for the model. Rearranging the leakage flow rate equation (2.21) to solve for orifice area results in the following

$$A = \frac{Q_{leakage}}{C_d\sqrt{2P/\rho}} \tag{2.24}$$

where C_d is the orifice discharge coefficient equal to 0.7, ρ is the fluid density of mineral oil, and P is the pressure difference across the cylinder. The pressure difference was the check valve cracking pressure minus the pressure of the rod-side which was the pressure of the check valve and pressure to lift the load. Because the leakage area was dependent on pressure across the cylinder and piston speed, there was a different value for every test point. The values for each set of speeds regardless of pressure were similar enough that their average was used. The values found are listed in Table 2.4.

The load force on the rod is less than the pressure times the area of the piston because of the friction in the cylinder and the pressure on the cap-side. Cylinder force efficiency was calculated by

$$\eta_p = \frac{F_{load}}{P_R A_R} \tag{2.25}$$

where F_{load} is the rod load force, P_R is the rod-side pressure, and A_R is the rod-side cylinder area[37]. Because of volume difference between the cap-side of the cylinder

Speed (rpm)	Load (lbf)	Orifice area (m^2)	Simulation area (m^2)
2000	105	1.4e-7	1.39 e-7
	80	1.37e-7	
	55	1.38e-7	
1400	105	1.09e-7	1 e-7
	80	1.05e-7	
	55	1.025e-7	
800	105	6.6e-8	6e-8
	80	5.8e-8	
	55	4.8e-8	

Table 2.4: *Leakage flow described by flow through an orifice of the experimentally calculated area.*

and the rod-side of the cylinder, a check valve was needed on the cap-side to relieve the extra fluid that was being forced out of the cap-end. The check valve cracking pressure parameter was an experimental parameter that could be set. A comparison of check valve cracking pressure versus force efficiency of the cylinder was done. Here the cracking pressure of the check valve set the cap-side pressure and rod-side pressure was a response to the load using (2.18).

2.5 Data Collection

The hardware prototype system was operated under different conditions and steady-state system results were found that could be compared to the model. The power transmission alone was analyzed without the AFO shell by mounting it vertically and using the piston to lift weight, Fig 2.8. The results were found by applying weight (50, 80, 105 lbf) at the end of the piston of the cylinder and recording both the pressure in the rod-side of the cylinder and piston speed while retracting the piston at different set motor speeds (800, 1400, 2000 rpm). A pressure sensor on the rod-side was used to measure pressure while piston retraction was recorded with a linear potentiometer. The voltage data from the linear potientometer was converted to position and then differentiated into piston velocity. The data acquistion system recorded linear potientometer voltage and rod-side pressure sensor voltage in real-time at 100 Hz. The data was collected with the piston running in the retraction direction because this was the direction needed

for plantarflexion which demands more force than dorsiflexion as well as being more inefficient than piston extension. The prototype was run using mineral oil as the system fluid.

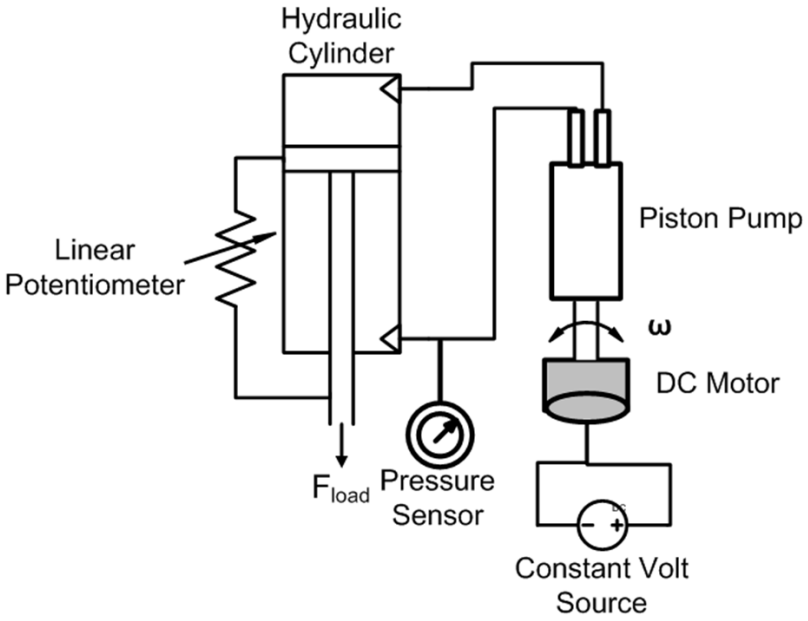

Figure 2.8: *The HAFO was tested with a weight applied at the piston and a commanded motor shaft speed. The piston velocity was recorded with a linear potentiometer and system rod-side pressure was recorded with a pressure sensor.*

2.6 Model prototype comparison

To validate the model, a series of simulations was run with parameters matching the hardware prototype at the same five shaft speeds and applied forces. The simulation results must match the prototype results to validate that the model can be used to drive future designs.

Chapter 3

Results

3.1 Mapping Ankle Function to Requirements

Using the inverse design method, design requirement results were calculated. By using the data from [2] shown in Fig. 1.2, the requirements of each component of the power transmission could be found for the whole gait cycle. The method was used to decide the moment arm length, pump displacement, and motor size. Because moment arm length comes first in the power transmission after the ankle dynamics, the whole method was employed to decide which length was more appropriate.

Applying (2.1) and (2.2) to the ankle data and using two possible moment arms, a short 10 cm and a long 14 cm, the data in Fig. 3.2 was found. The curves represent the output from the piston, force and linear velocity. The curves follow the same pattern as the input data because the cosine of the ankle angle is close to one. This means that force peaks with ankle torque during the gait needing a maximum force at the push-off. And the velocity demands track the same pattern as well. The configuration with the larger moment arm requires less force to be applied at the moment arm but does require more velocity than the smaller moment arm. The power of the system is not dependent on the moment arm because power is conserved in the system as is seen by multiplying (2.1) and (2.2) together to get power, the moment arms cancel out.

Fig. 3.3 shows plots of pressure and flow rate from the pump calculated from (2.3) and (2.4) using the force and velocity from the piston, Fig 3.2, and the area of the 1.0625 inch diameter bore cylinder. The pressure needed in the system with the 10 cm

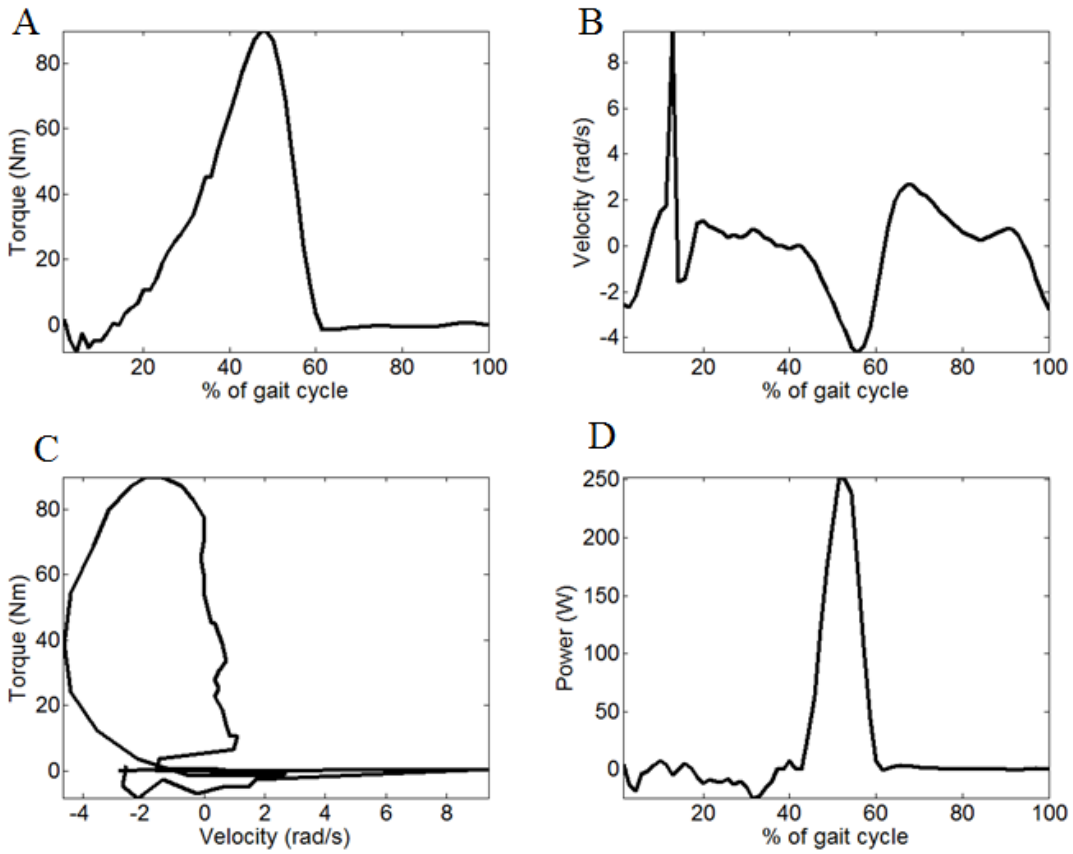

Figure 3.1: *Ankle Dynamics from [2]. A) Torque required throughout the gait cycle. B) Velocity required throughout the gait cycle. C) Torque needed versus velocity needed. D) Power required at the ankle throughout one gait cycle.*

moment arm is 2.4 MPa while the pressure in the system with the 14 cm moment arm is 1.5 MPa.

From pump pressure and flow rate with a pump displacement of 0.4 cc/rev, the motor torque and speed were calculated using Equations (2.5) and (2.6). These are displayed in Fig 3.4. The pump displacement affected both equations and the resulting motor torque and velocity have corresponding trends to the pressure and flow rate. The maximum motor torque needed is 0.2 Nm with a smaller moment arm and 0.15 Nm with the larger moment arm.

The battery supplies current and voltage to the motor so that it can supply the necessary torque and speed. The current and voltage that the motor needs in order to

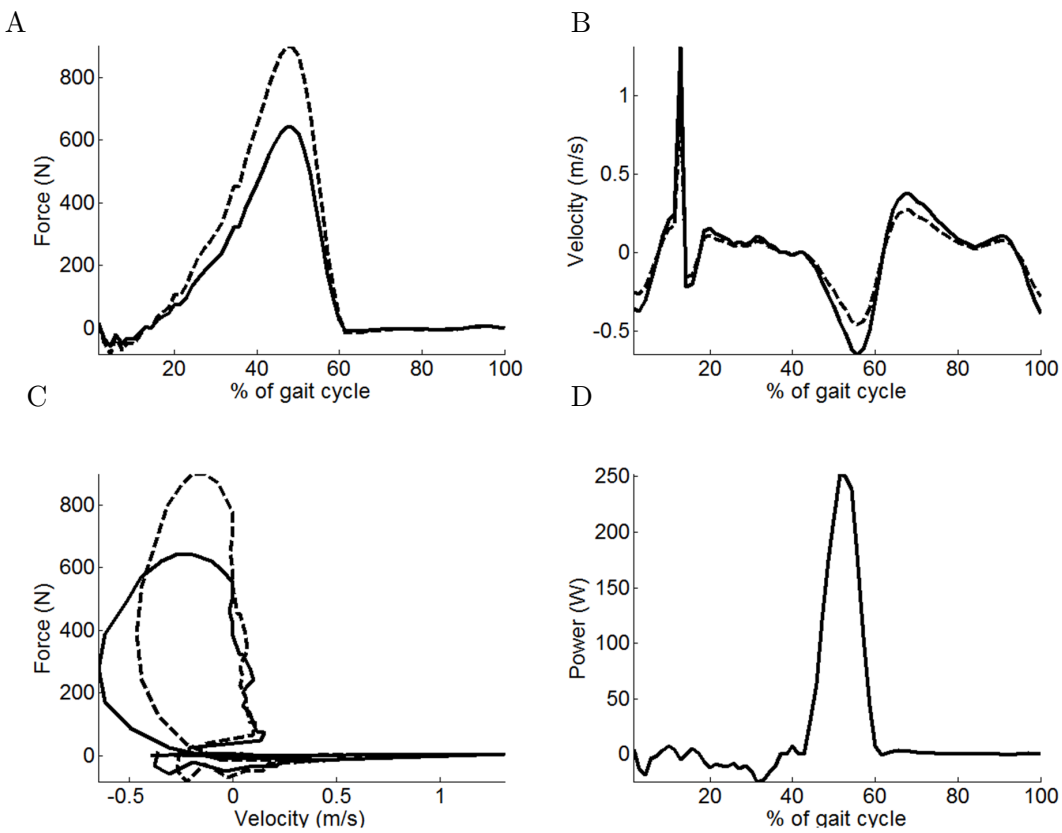

Figure 3.2: *Force and velocity at cylinder piston, 10 cm moment arm (dashed) and 14 cm moment arm (solid). A) Force required throughout the gait cycle. B) Velocity required throughout the gait cycle. C) Force versus velocity needed. D) Power required in the battery throughout one gait cycle.*

provide the torque and speed were calculated using Equations (2.7) and (2.8) along with the motors torque constant of 36 mNm/A and speed constant of 600 rpm/V, and are shown in Fig 3.5. Here the same motor is being compared so power needed is the same, but current requirements are different. A 7 A peak current is needed for the smaller arm while 5 A are needed for the larger moment arm.

The method can be used to find the requirements of the motor and the battery depending on the size of the pump and motor. The two available small piston pumps, Takako's micro axial piston pump and Parker Hannafin Oildyne's cartridge piston pump, have different displacements, 0.4 cc/rev and 0.21 cc/rev. These were compared using Equations (2.5) and (2.6) to see how the motor would need to respond to create the

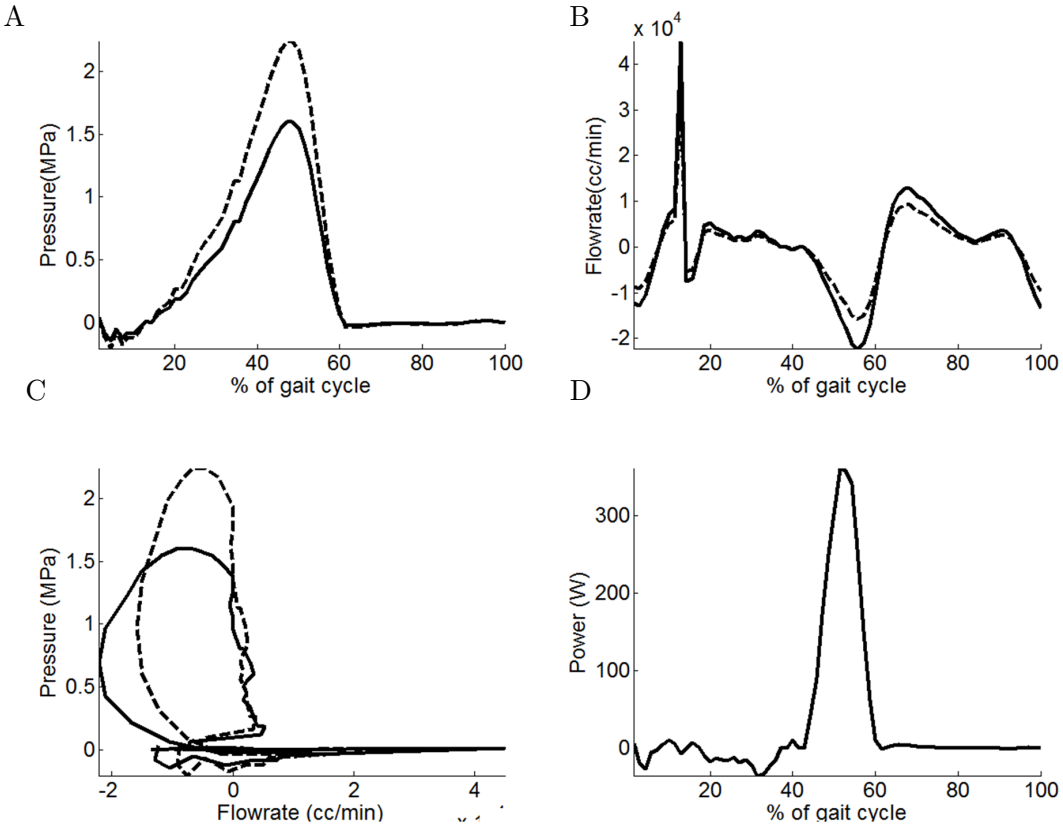

Figure 3.3: *Pressure and flow rate out of the pump, 10 cm moment arm (dashed) and 14 cm moment arm (solid). A) Pressure required throughout the gait cycle. B) Flow rate required throughout the gait cycle. C) Pressure versus flow rate needed. D) Power required at the pump throughout one gait cycle.*

necessary flow and pressure from the pump. Fig 3.6 shows the necessary motor outputs for these pump choices; for a large pump displacement the motor torque maximum is .07 Nm while a smaller displacement pump needs 0.15 Nm. The smaller displacement pump does have a faster flow rate and therefore a faster motor shaft speed.

The motor chosen for the prototype was compared to another motor to understand its power needs. The motor (Maxon 370426) used in the prototype had a torque constant of 35.7 mNm/A and a speed constant of 268 rpm/V, while a similar motor (Maxon 339286) had constants of 47.5 mNm/A and speed constant of 201 rpm/V. Battery voltage and current supplied to these motors is shown in Fig 3.7. The 370426 required 5.5 A and 400 V to operate in the system with a 14 cm moment arm. The 339286 needed 4 A

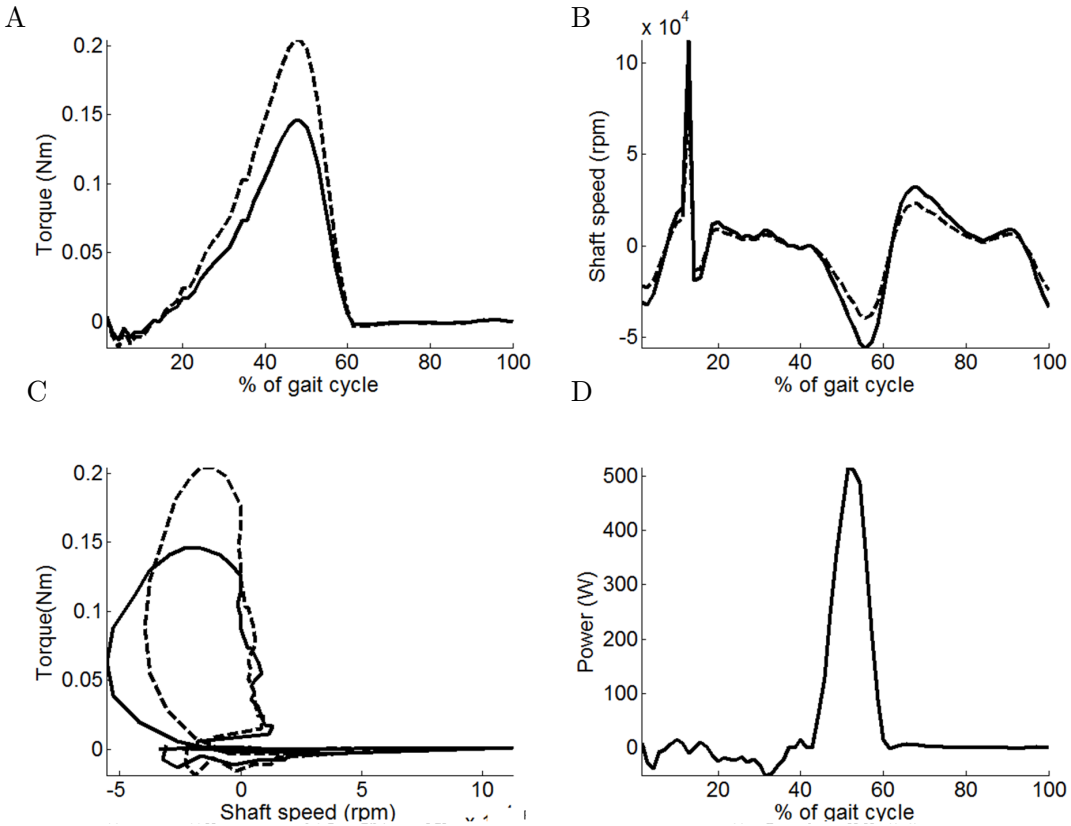

Figure 3.4: *Torque and speed out of motor, 10 cm moment arm (dashed) and 14 cm moment arm (solid). A) Torque required throughout the gait cycle. B) Velocity required throughout the gait cycle. C) Torque needed versus velocity needed. D) Power required at the motor throughout one gait cycle.*

and 700 V. These voltage requirements exceed the maximum supply voltage of the motors and require a high power input. By conservation of power each component requires ankle power multiplied by the efficiency of the component therefore both motors have the same power need while having differing voltage requirements. Looking at system efficiencies, the battery must supply enough power to overcome all system inefficiencies and still supply ankle power at the ankle. The more efficient the system is, the less power is needed at the battery which allows the design to use a smaller battery.

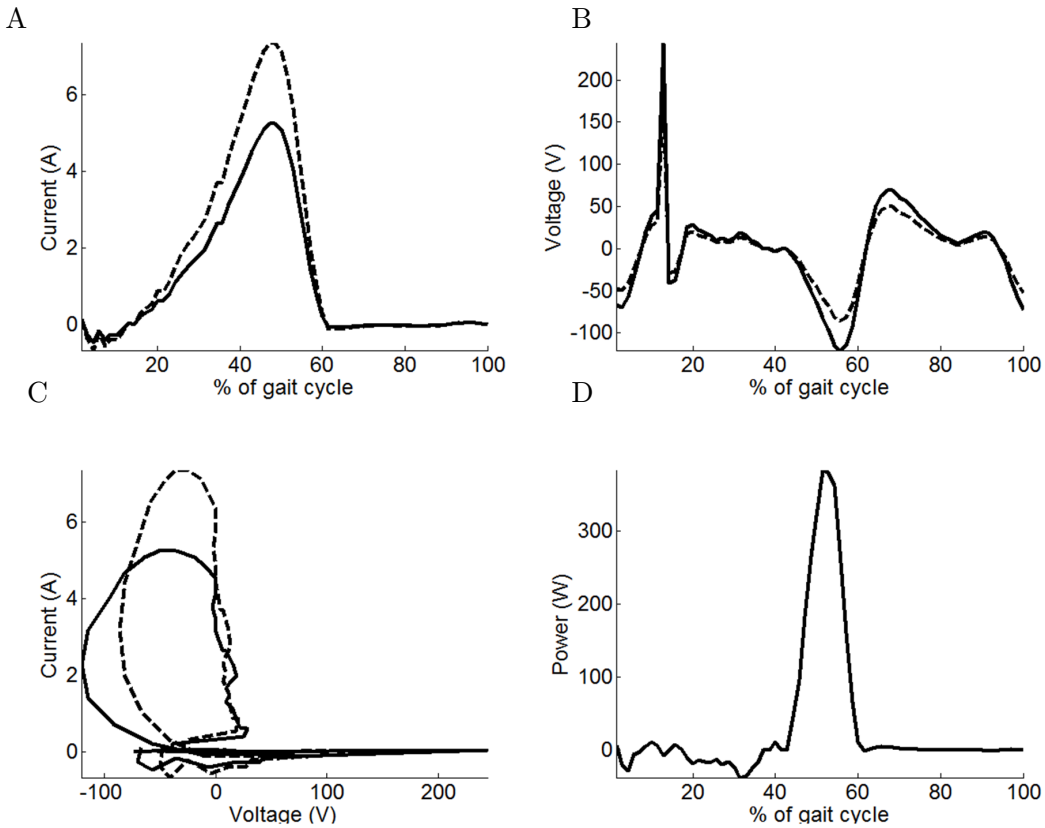

Figure 3.5: *Current and voltage out of battery, 10 cm moment arm (dashed) and 14 cm moment arm (solid). A) Current required throughout the gait cycle. B) Voltage required throughout the gait cycle. C) Current versus voltage needed. D) Power required at the battery throughout one gait cycle.*

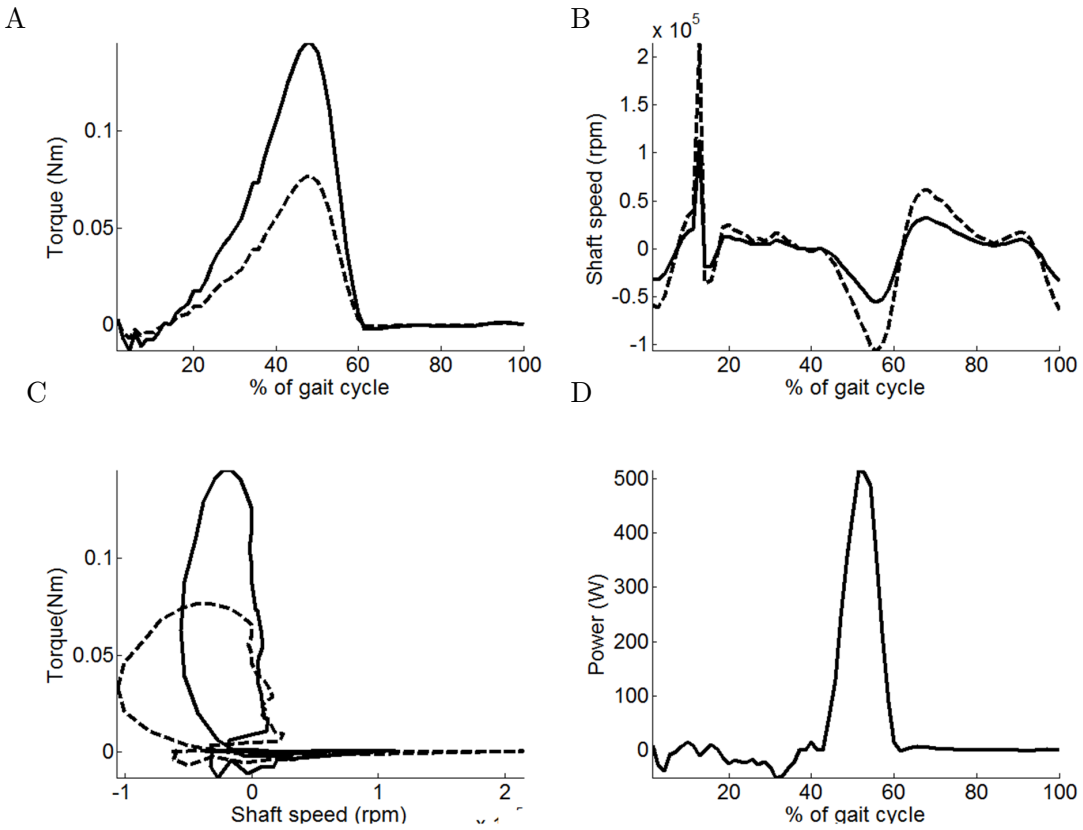

Figure 3.6: *Torque and speed out of motor, using 0.4 cc/rev (solid) and 0.21 cc/rev (dashed) pump displacement. A) Torque required throughout the gait cycle. B) Velocity required throughout the gait cycle. C) Torque needed and velocity needed. D) Power required at the motor throughout one gait cycle.*

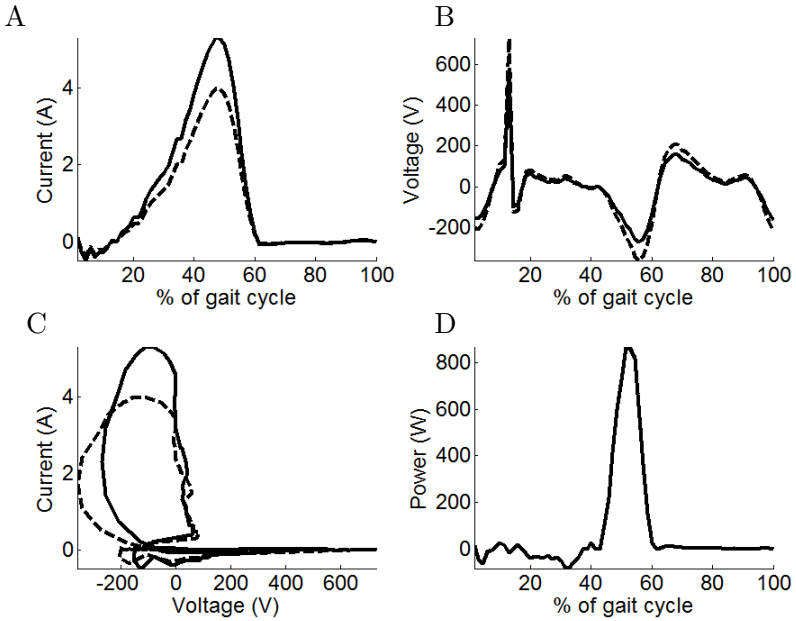

Figure 3.7: *Current and voltage out of battery, comparing two motors, Maxon 370426 (solid) and Maxon 339286 (dashed). A) Current required throughout the gait cycle. B) Voltage required throughout the gait cycle. C) Current and voltage needed. D) Power required at the battery throughout one gait cycle.*

3.2 Dynamic Equations

The system must follow the conservation of mass and momentum described by the dynamics in (2.10) and (2.9). These equations were used as an initial check of the object-oriented approach of the model built in SimHydraulics see Fig. 3.8. The object-oriented model was simulated recording the cylinder rod-side and cap-side pressure. The differential system equations were solved for the cylinder rod-side and cap-side pressure using the measured piston velocity and flow rate from the simulations and a series of transfer functions [37]. The model results matched the dynamics equations.

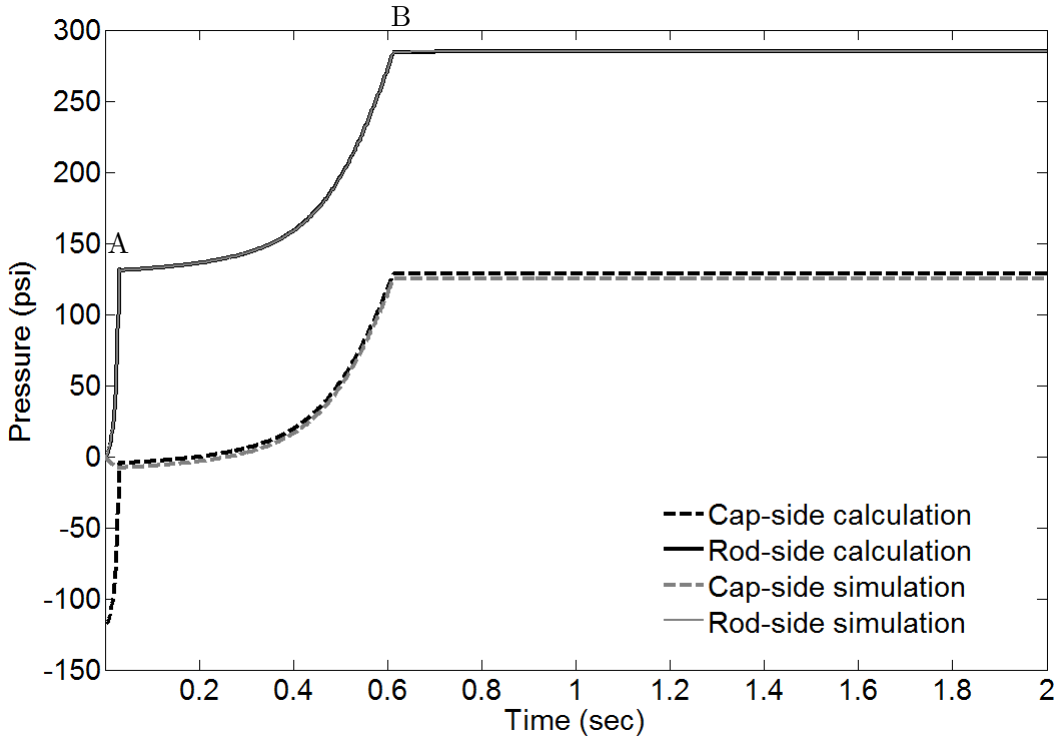

Figure 3.8: *Comparing the SimHydraulics model results to the dynamics equations* (2.10) *and* (2.9). *The solid lines are the pressure outputs on the rod-side of the cylinder while the dashed lines are the outputs for the cap-side. Point A is the lifting pressure where the load begins to move. Point B is steady-state pressure where the check valve has opened to relieve excess pressure. The results from the simulation of the model match the calculations.*

The model was used to understand the transient behavior seen in Fig. 3.8. The

system does not instantaneously reach the desired pressure but rather goes through two transition phases. These transitions are due the check valves on each side of the cylinder (Fig. 2.3). These were necessary because of the volume differences in the two sides of the double acting cylinder. Because the system uses one side of the cylinder as a tank while pressurizing the other and vice versa, the volume and flow rate from the tank side must be equal to the demands of the pressure side. This means extra volume must be relieved when flow goes to the rod-side and extra volume must be drawn in when flow goes to the cap-side. The first pressure transient was the pressure rise to reach lifting pressure A equal to the load divided by the cylinder area; where the load equals 467 N, the heaviest experimental force applied, and the cylinder area is the prototype cylinder area. The pressure continues to rise until the cap-side pressure reaches the check valve cracking pressure of 125 psi at which point the rod-side pressure B was equal to the solution of (2.10).

Results from simulation of the model were used to illustrate the need for these valves by examining the pressure on the rod-side with a tank on the cap-side, Fig. 3.9, and with no tank and no check valve on the cap-side, Fig. 3.10. With a tank on the cap-side, the excess fluid volume was relieved without any pressure loss. The rod-side pressure was equal to the load force over area of the piston cap on that side, where the load equals 467N, the heaviest experimental force applied. With no way to relieve excess fluid it builds up creating an ever increasing pressure seen in Fig. 3.10.

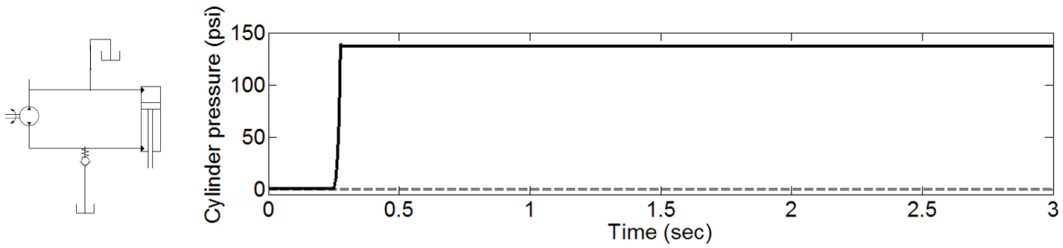

Figure 3.9: *With a tank on the cap-side, all excess flow is relieved from the system and the cap-side pressure (dashed) is zero and the rod-side pressure (solid) is related to the load. Here the applied load is 467 N while the cylinder parameters are from Table 2.3.*

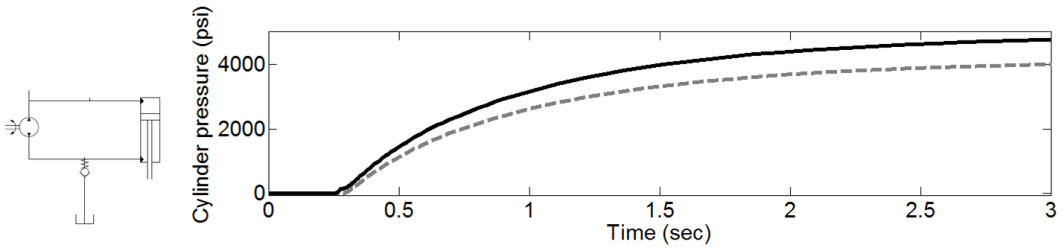

Figure 3.10: *With no check valve to relieve excess flow on the cap-side, the volume of excess fluid increases and the pressure in the system increases. Here the applied load is 467 N while the cylinder parameters are from Table 2.3. Cap-side pressure (dashed) and rod-side pressure (solid).*

3.3 Determining Component Parameters

The model parameters were obtained from experimental analysis on the hardware components described in Section 2.4.

3.3.1 Pump Parameters

The Takako axial piston pump (TFH-040) was tested, and torque-pressure and flow rate-speed curves were found. The experimental volumetric efficiency was 99% and the mechanical efficiency was 62-76% based on the flow rate of the system (Section 2.4.2). A simulation was run using the experimental efficiency values in (2.14) and (2.16) and compared to the system in Figs 3.11 and 3.12. The total efficiency of the model was the multiplication of mechanical and volumetric efficiencies. The model assumes that leakage flow is proportional to the pressure differential across the pump. The leakage equation, (2.15), is specified only at nominal values of pressure, speed, and volumetric efficiency. From the maximum settings of the Takako pump, the pressure and speed were 2000 psi and 2000 rpm. Experimental and simulated efficiency are compared in Fig 3.13. The experimental pump efficiency was found at several points by calculating power in and power out. The simulated pump efficiency was found by data-fitting the experimental data set. The experimental results showed that the pump had minimal leakage and was suspectible to flow dependent pressure values. The flow-speed curves were well matched from the model and the experiment. The total efficiency experimental

points were scattered around the curve of simulated efficiency with an overall total efficiency of 73% when the power is greater than 75W. At the 50W operating power of the motor, the modeled pump efficiency was 65%.

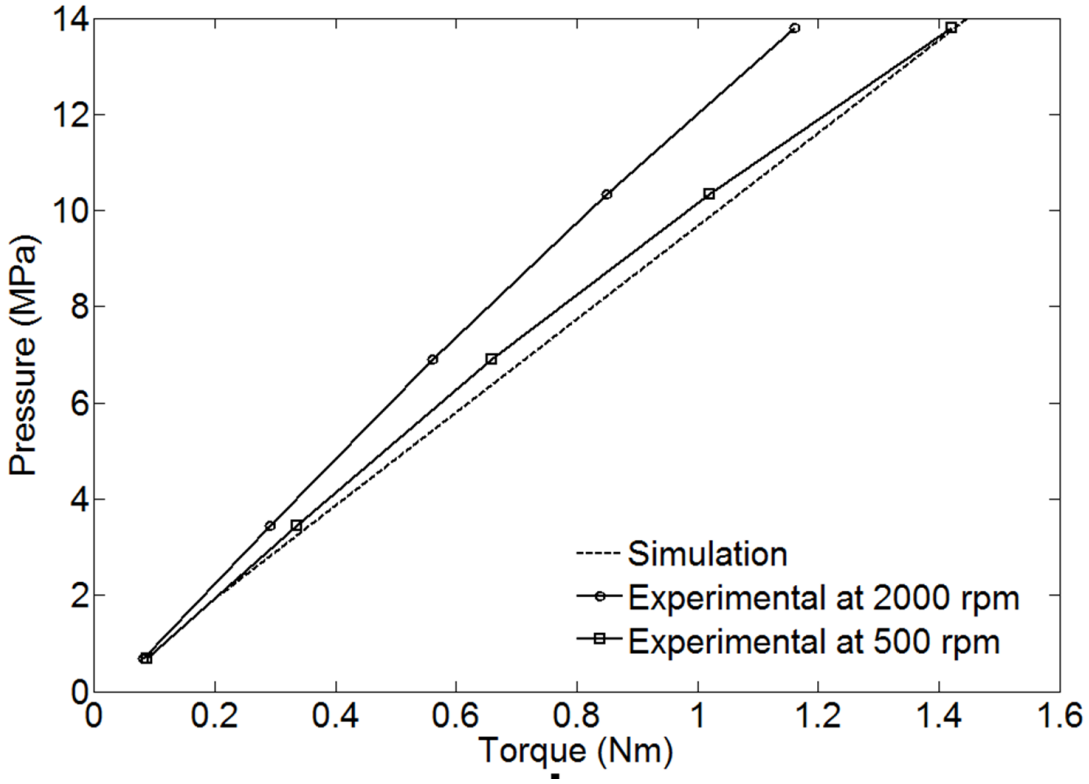

Figure 3.11: *Torque-pressure curves for axial piston pump; model (dashed) and experimental system (solid) at 2000 rpm and 500 rpm.*

3.3.2 Motor Parameters

Fig 3.14 shows the simulated torque-speed curves from the model and the experimental curves in both the clockwise and counterclockwise direction. Because the motor was a motor plus a speed controller, these are flat curves that show the permissible steady-state operation ranges. The Maxon motor had a maximum speed of 4500 rpm in the clockwise direction and 5000 rpm in the counterclockwise direction. The maximum torque was between 0.12 Nm and 0.14 Nm.

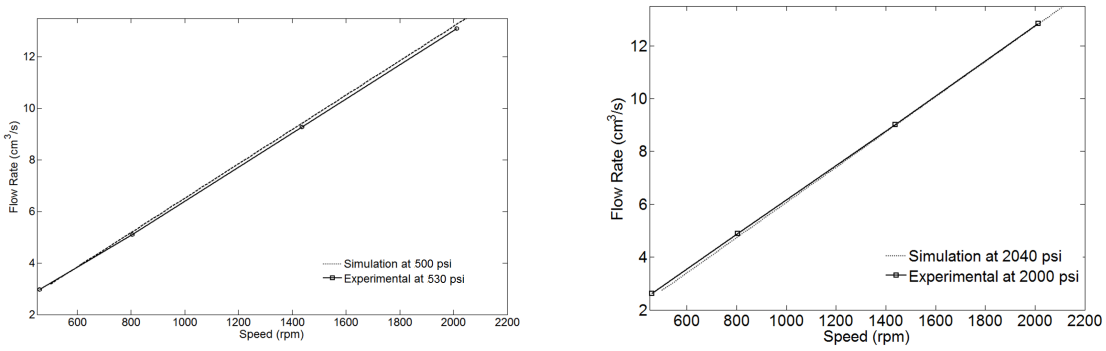

Figure 3.12: *Flow rate-shaft speed curves for axial piston pump (left) at 500 psi and (right) at 2000 psi.*

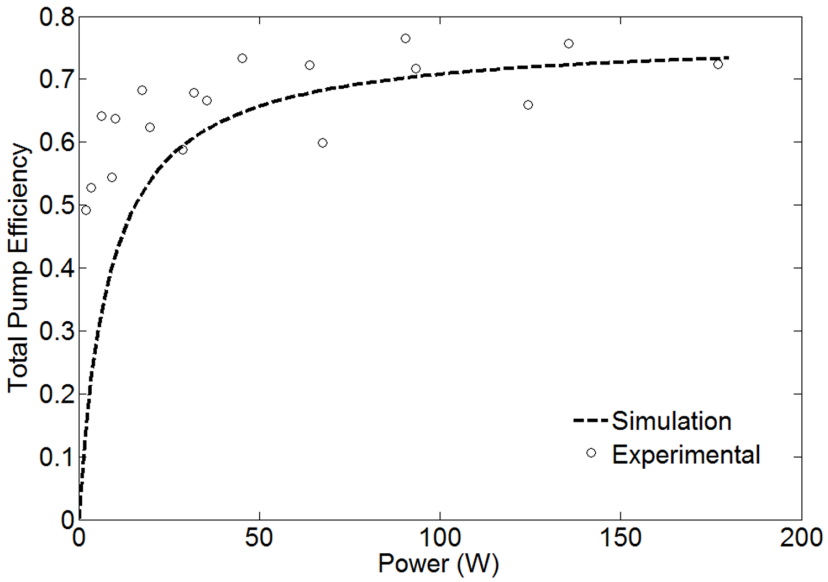

Figure 3.13: *Efficiency versus power output curves for axial piston pump with a nominal speed and pressure of 2000 rpm and 2000 psi; model (dashed) and experimental system.*

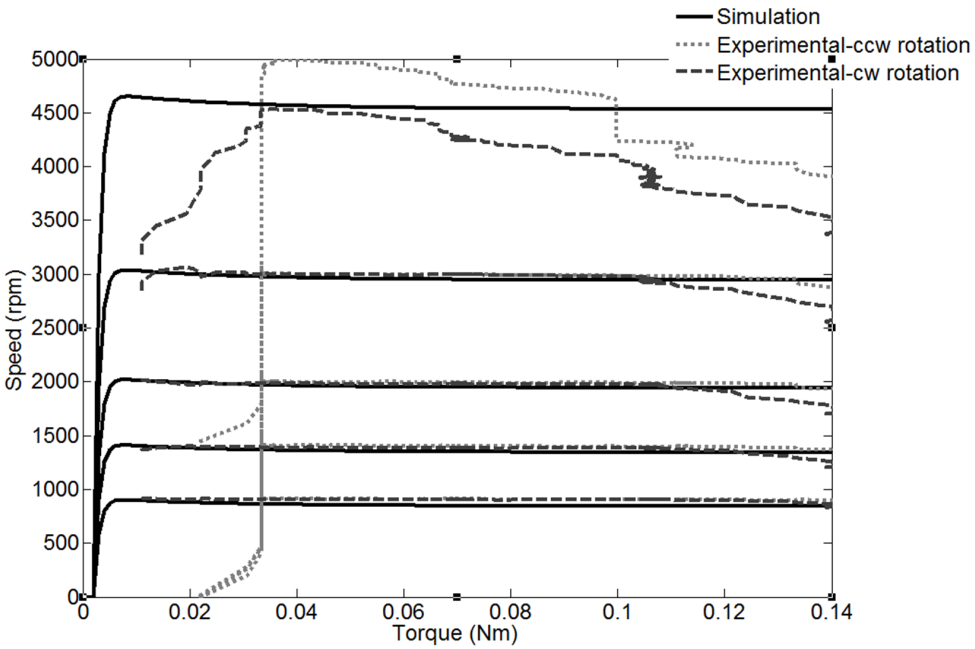

Figure 3.14: *Torque-speed curve for Maxon motor and speed controller (solid) model and experimental system (dashed) with clockwise and counterclockwise rotation denoted.*

3.3.3 Cylinder Leakage Parameters

Cylinder leakage was modeled as a parallel orifice to the cylinder. The area of this orifice was set according to the previously described method in Subsection 2.4.3 and the values found are listed in Table 2.4. A simulation of the model was run with the values in the table as well as the experimental parameters of the pump and motor, and the plots of piston velocity are shown for each set experimental speed in Figs 3.15 through 3.17. The simulation of the model can track the steady state speed, but the control loop was not tuned to match the rise rate.

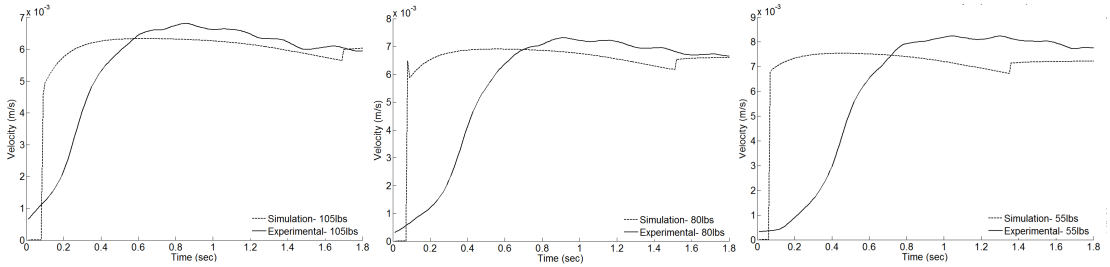

Figure 3.15: *Comparing the simulation's piston velocity at a commanded speed of 800 rpm to the experimental results under three different loads.*

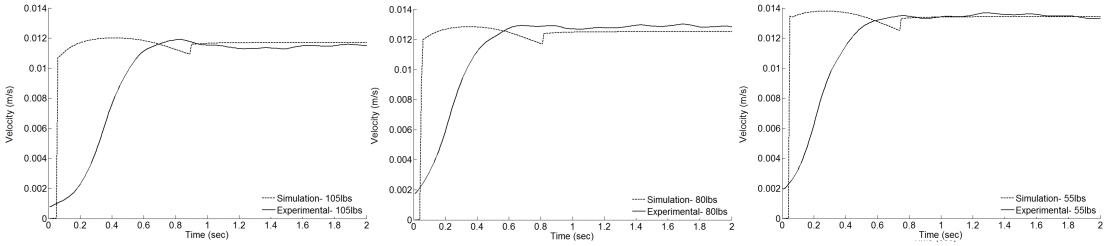

Figure 3.16: *Comparing the simulation's piston velocity at a commanded speed of 1400 rpm to the experimental results under three different loads.*

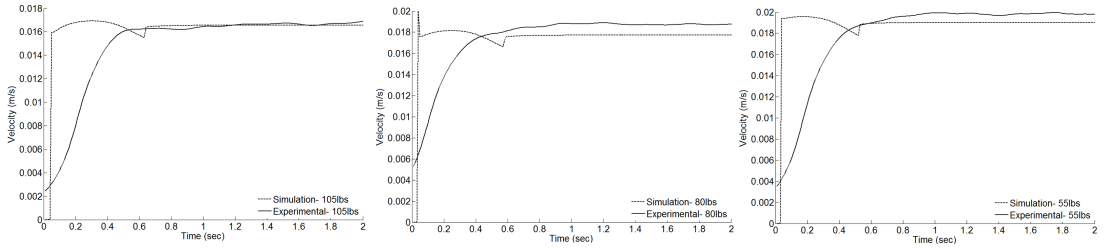

Figure 3.17: *Comparing the simulation's piston velocity at a commanded speed of 2000 rpm to the experimental results under three different loads.*

3.4 Model Validation

The model was fit with the same parameters as the hardware components, Table 2.3, and the hardware testing was simulated by applying a constant speed to the motor and a constant force to the piston. The pressure in the system was recorded at the rod-side of the cylinder to replicate the hardware prototype testing. The simulated output pressure for each applied force was plotted at different commanded speeds to compare to the hardware output in each of Figs 3.18 through 3.20. The model compares to the prototype data at the steady state value of pressure but the rise rate varied. The lighter loads rose faster in the model than the experiment regardless of commanded speed.

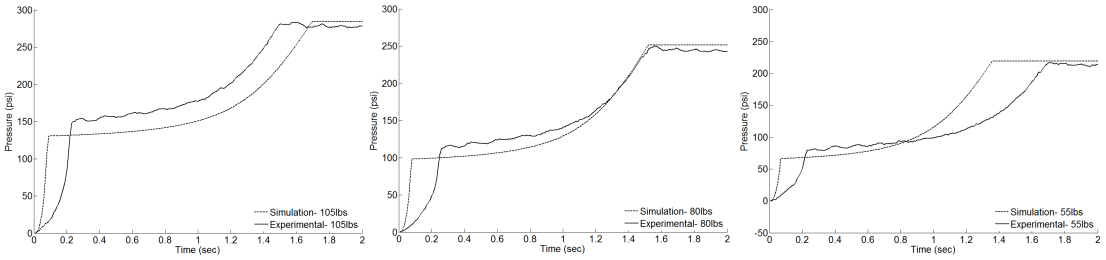

Figure 3.18: *Comparing the simulation's rod-side pressure at 800 rpm and varying loads to the experimental results.*

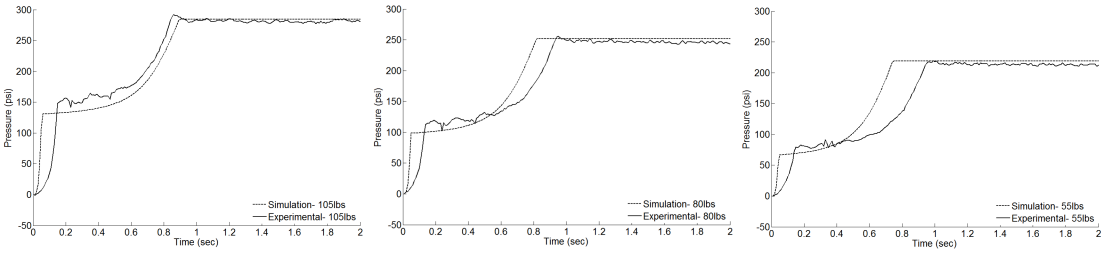

Figure 3.19: *Comparing the simulation's rod-side pressure at 1400 rpm and varying loads to the experimental results.*

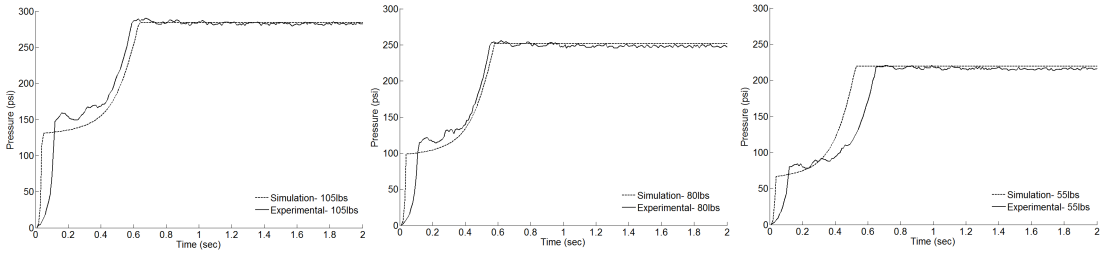

Figure 3.20: *Comparing the simulation's rod-side pressure at 2000 rpm and varying loads to the experimental results.*

3.5 Model Exploration

The model was evaluated and used to answer the objectives listed in Section 2.2.5. The first objective of understanding system behavior was verified in Section 3.2.

The purpose of this power transmission is for use in a powered ankle-foot orthosis. For this to be met, the system must meet the desired gait parameters as stated in the second objective of Section 3.2. The simulated output at the AFO was a rod-side cylinder pressure and a piston velocity. The pressure is a result of the force on the piston, which was applied via a moment arm at the ankle and caused by ankle torque. The maximum force on the piston corresponding to the gait cycle was shown in Fig. 3.2 to be 600 N. The corresponding simulated system pressure was 319 psi on the rod-side of the cylinder. The maximum piston velocity in Fig. 3.2 was 1.25 m/s. The corresponding motor speed needed was 90,000 rpm. This speed is not attainable with a real motor showing that our prototype is incapable of gait parameters. Having a better understanding of the sytem from the model will give an understanding of which parameters to change to give a lower motor speed.

The third objective was satisfied by using the model to determine the effect of component properties on the system's performance. The volume differences of the cylinder ends were compensated for by including check valves in the system. Because pressure is needed to open the cap-side check valve, the system must create additional rod-side pressure beyond what is needed to move the load. Having to create this additional pressure causes the system to be inefficient. A simulation of the model was done operating under different check valve cracking pressures to demonstrate the change in efficiency calculated by using (2.25), the applied load, and the rod-side pressure. Results in

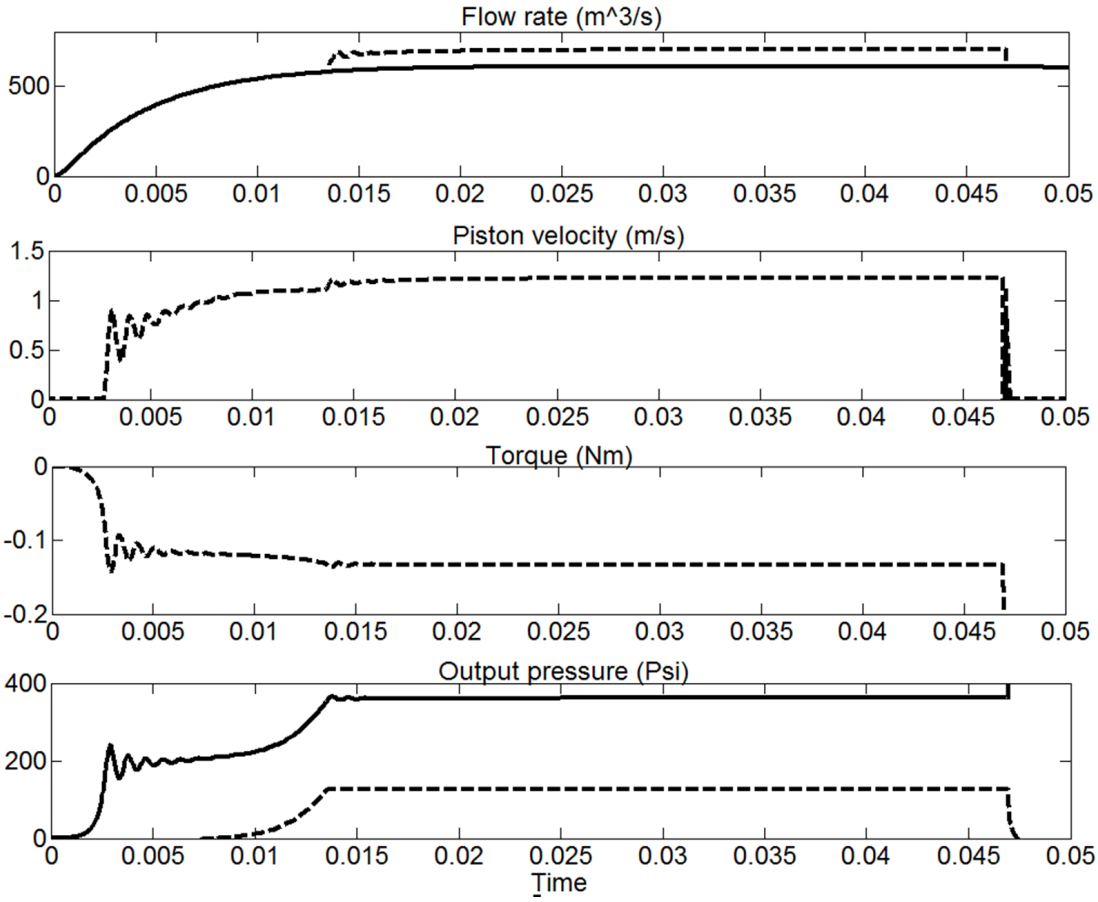

Figure 3.21: *Using the maximum load and the needed velocity of the gait cycle, the system performance requirements are a maximum pressure of 319psi and a motor speed of 90,000 rpm, corresponding to the 600 m^3/sec flow rate. Flow rate was recorded before the check valve (dashed) and after the check valve (solid). Pressure was recorded at the rod-side (solid) and cap-side(dashed).*

Fig. 3.22 show that the value of cracking pressure has an effect on the efficiency. A lower check valve cracking pressure of 50 psi makes the system perform more efficiently at 70% compared to the prototype cracking pressure of 125 psi which created a system with 50% efficiency. As described earlier the system needs a check valve to operate in both directions. The check valve cracking pressure must allow the cap-side pressure to reach a value that causes extension of the cylinder and dorsiflexion of the ankle.

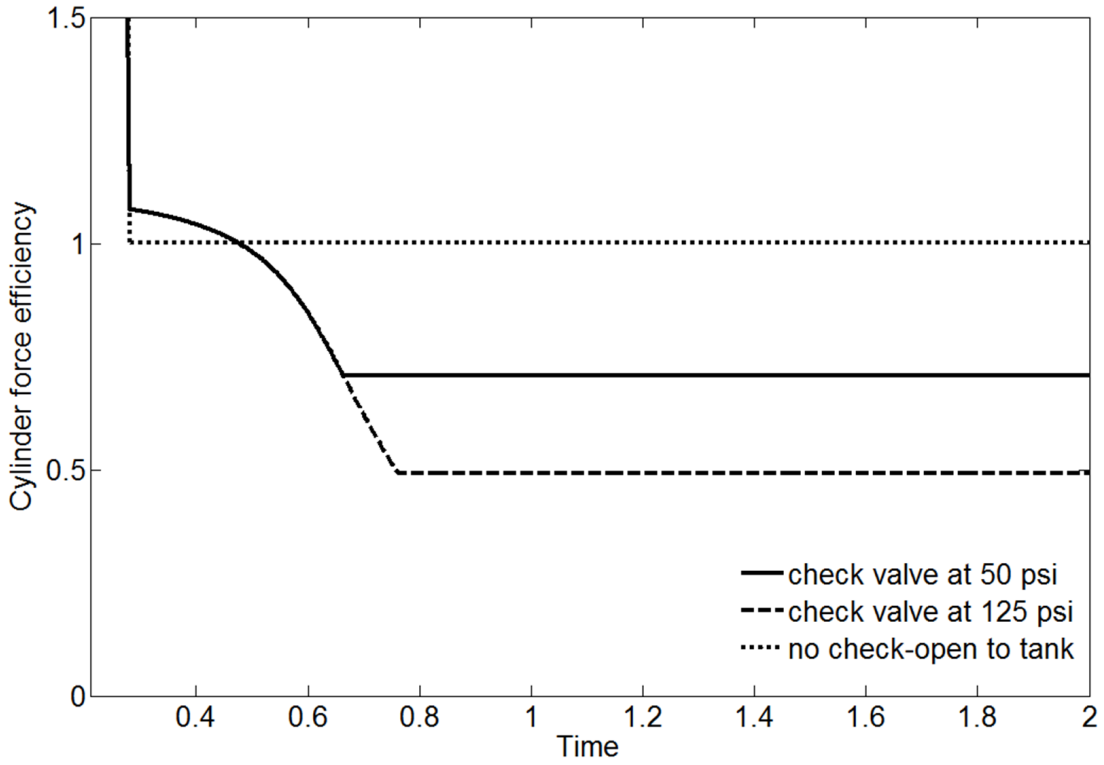

Figure 3.22: *The check valve opening pressure setting determines how much system pressure must be created before relieving the excess fluid from the cap-side, the larger the pressure the more inefficient the cylinder becomes.*

The dimensions of the components are important when designing the power transmission especially as design plans move into custom fabricated parts. The bore size of the cylinder affected the efficiency of the system calculated by (2.25) and the system as seen in Fig 3.23, a smaller bore cylinder of a half inch diameter was less efficient at 20% with the same applied load compared to the prototype cylinder with a 1.0625" diameter and 50% efficiency.

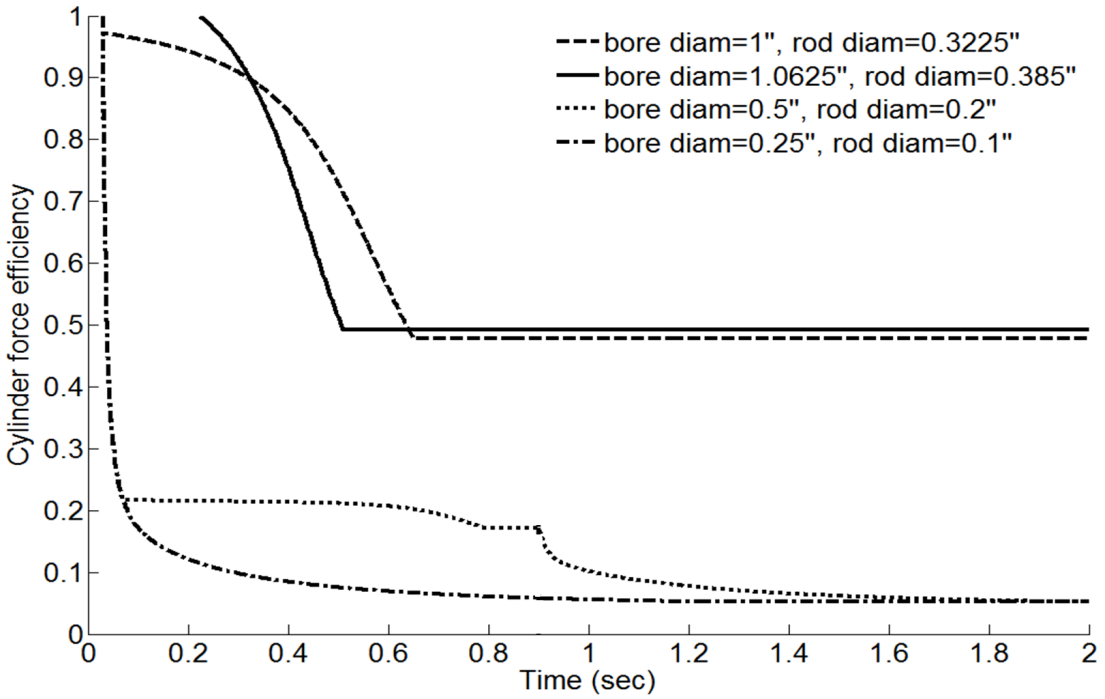

Figure 3.23: *The size of the bore diameter effects the pressure needed to lift a specified force, the smaller diameter the more pressure is needed to lift the same force and this larger pressure creates a more inefficent system.*

Other properties such as pump displacement affected both force and velocity outputs of the pump. When commanded motor speed and piston load force are kept constant, a smaller displacement resulted in a lower flowrate and a lower shaft torque in Fig. 3.24, where lower flow rate resulted in lower piston velocity.

Understanding the affect of fluid properties on the system satifies the fourth objective of Section 3.2. Theoretically hydraulic power is transmitted through an incompressible fluid, however the type of fluid has an effect on the performance of the system. Bulk modulus is the measure of the incompressibility of the fluid. Bulk modulus affects the pressure characteristics as well as velocity of the system. Changing the bulk modulus was simulated and is shown in Fig. 3.25. A higher bulk modulus resulted in less time spent compressing the volume of fluid, and the system reaching steady state pressure sooner and maximum flow rate being reached sooner than with a lower bulk modulus.

Fluid density and viscosity affected flow velocity. A low density fluid causes a lower

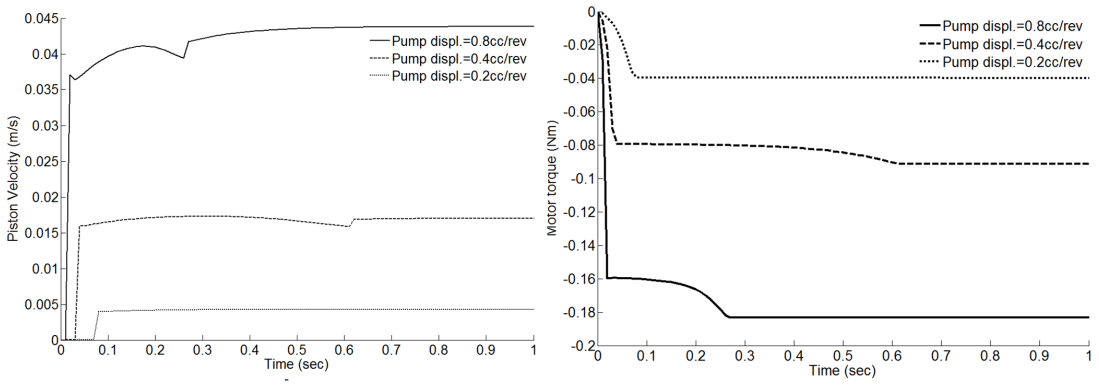

Figure 3.24: *The amount a pump displaces per revolution affects the amount of fluid moved per second and the pressure created, thus a lower displacement results in a lower flow rate and less motor torque needed to create the required pressure. The sign of the torque is arbitary, here is signifies that motor's negative rotation is causing piston retraction.*

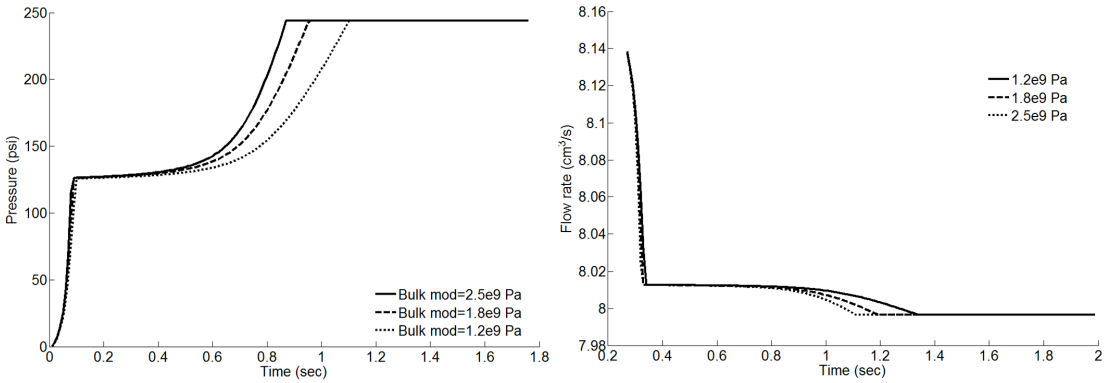

Figure 3.25: *An incompressible fluid has a high bulk modulus resulting in less time spent compressing the volume. This means the desired system pressure and flow rate are reached sooner than with a more compressible fluid.*

flow rate, and a low viscosity fluid causes a lower flow rate, Fig. 3.26. This loss is seen in (2.14) where the leakage coeffecient contains both density and viscosity. A less viscous and less dense fluid will leak more causing less shaft speed to be converted to flow rate in the pump.

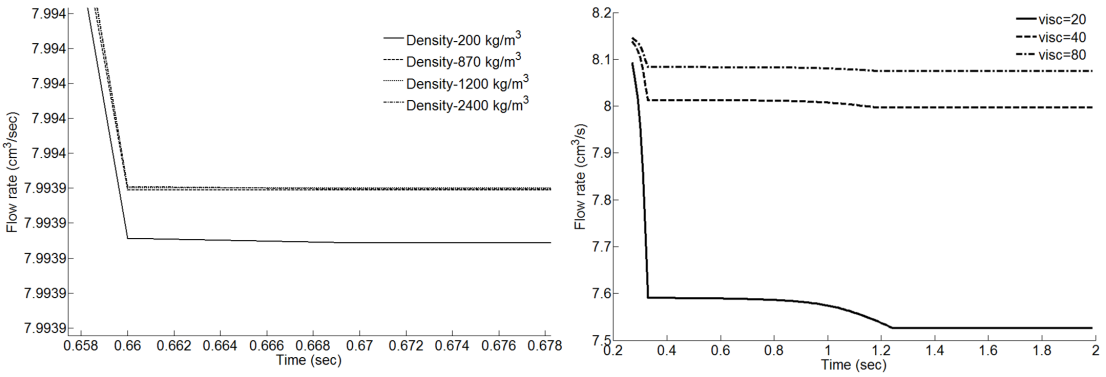

Figure 3.26: *A low density and viscosity cause a fluid to have a smaller flow rate out of the pump due to fluid leakage described in* (2.14).

Chapter 4

Discussion

4.1 Design Requirements Method

The method derived in Section 2.1 for developing design requirements can be used to look at the requirements for the components throughout the gait cycle. The method was used to show that by knowing the requirements of the driven component the requirements of the driving component can be found. Applying the general principles of each component to the known needed torques and velocities found the required forces and velocities of the powering component. The limitation of using general principles was the inability to account for efficiency and complex geometries. This combined with a simple control method meant that the experimental prototype would not track the results of the design requirements method exactly. The advantage then was that the method was useful for comparing components and parameter values in a straightforward way.

The method with parameters set to match available off-the-shelf components was used to demonstrate that these components could actuate the AFO. With a 14 cm moment arm at the ankle, the cylinder piston needed to provide 600 N of force with a maximum velocity of 1.5 m/s. The buckling load of the prototype Bimba cylinder rod (assuming stainless steel construction) is 494 kN which is well above the force needed. The high velocity might be troublesome for the cylinder seal since a tight seal would leak less at low speeds but have increased friction force during high speed. The specific seal material is unknown from the data sheet. The shorter moment arm (10 cm) needs a higher force and lower velocity; a higher force will cause the motor torque to be

unachievable.

To achieve the 1.5 m/s a 40,000 cc/min flow rate was needed. This is the limiting factor of the prototype design. A 40,000 cc/min flow rate, see Fig. 3.3, requires a motor speed of 10,000 rpm. DC motors are capable of this speed. Currently available small hydraulic piston pumps are generally limited to 2,000 rpm. The DC Maxon motor used in the prototype had a limit of 4,500 rpm. The prototype then is limited to slow speed operation due the hydraulic pump's limitations. The prototype needs a faster running pump to provide full ankle kinetics.

The pressure needed to create a 600 N force was 1.5 MPa which is well under the Bimba cylinder's pressure rating of 3.4 MPa. The torque provided by the motor to the pump to achieve this 1.5 MPa is 0.15 Nm, which is under the motor's 0.154 Nm maximum torque limit. Using a shorter moment arm would require less motor speed, but more torque from the motor than the prototype motor is capable of providing.

The battery provides power to the motor and thus the system. The method shows that the current requirement for the longer moment arm is 5 A and the voltage needed is 225 V. The maximum supply voltage of the motor is 29 V so again the speed of the device is limited. With a shorter arm, the current is 4 A and the voltage needed is 600 V. During system tests, a voltage supply was used to avoid current drain of the battery that would decrease force in the system.

The design method was also used to compare pump displacements showing the difference between a 0.4 cc/rev pump and 0.21 cc/rev pump in Fig. 3.6. The torque needed from the motor to create the necessary pressure from the pump was halved using half the pump displacement, but the speed was then doubled. This method then can be used to see how this affects the battery requirements showing that the current requirement is again halved but the voltage needed is doubled.

Fig. 3.7 shows that motor constants affect the motors needed inputs from the battery. The comparison motor was a sister motor to the motor used in the prototype and needed much more voltage to provide the ankle requirements.

The method allows direct comparison of components however the limitation of the method is not being able to optimize the design over a range of chosen variables simultaneously. The method is too simplisitic. The simplicity of the method can be seen in Appendix A. The design of the method was meant to gain understanding of the general

principles rather than to calculate the most efficient system through linear optimization. A more complex linear optimization method would perform a search for combinations of parameters that met desired outcomes.

4.2 System Validation

4.2.1 Pump Testing

The piston pump model was more ideal than the experimental setup because it did not take leakage into account resulting in a pressure-torque curve that was not dependant on flow, but did track the experimental results well.

The flow-rate versus speed curve Fig. 3.12 was dependent on the pressure of the system. Bernoulli's principle states that a higher pressure will cause a greater flow. Using the efficiency found experimentally, the simulation was shown to represent the physical system.

The experimental efficiency data for the pump was scattered but could be fit with simulation data as shown in Fig. 3.13. The model inputs were total efficiency and volumetric efficiency. Total efficiency was found by multiplying the experimental values of mechanical and volumetric efficiencies. In the simulation for the model, this total efficiency was set at nominal speed and pressure values of 2,000 rpm and 2,000 psi. The results of the simulation followed the experimental behavior of the pump though the simulation had an ideal curve that started at zero efficiency at zero power output.

The model of the pump was satisfactory for the purpose of understanding its role as a power transformer given the complex nature of axial piston pumps and the relative simplicity of the equations used to model it. A complete model of an axial piston pump can be found here [43].

4.2.2 Motor Testing

The motor testing resulted in permissible steady-state operation ranges as seen in Fig. 3.14. The experimental data showed that the motor had a continuous torque range up to 0.14 Nm with clockwise rotation being weaker than counterclockwise. It is unclear if this discrepancy between directions is due to the testing equipment or the

motor. The speed range was a maximum of 4500 rpm with higher torques slowing down the motor. The simulated motor does not have a maximum torque because the PID controller feedback loop holds the speed at command speed regardless of torque output. The control loop increased supply voltage to control speed which did not give an accurate view of current draw so the motor model is over-simplified.

The motor model was satisfactory in replicating the experimental prototype motor though the model was not nearly as representative and complex as a brushless DC motor with speed compensation. The model can therefore be used to represent a variety of motors as long as testing is used to achieve the correct parameters.

4.2.3 Cylinder Leakage

Cylinder leakage was modeled as an orifice in parallel with the cylinder because the model assumed no leakage in the cylinder. Because no data sheet values were available on the leakage values of the cylinder used in the prototype, the leakage was inferred experimentally. Assuming any discrepancy between flow from the pump and flow moving the piston of the cylinder was lost to leakage, the area of this hypothetical orifice was found. This value was used in the simulation and the velocity of the piston in simulation was compared to the experimental velocity in Fig. 3.15 through 3.17. Because the model took flow lost to fluid compressibility and the volumetric efficiency of the pump into account, the assumption that the remainder of the flow that did not move the cylinder was lost to cylinder leakage seemed reasonable. The hypothetical orifice areas were reasonably small and represent all internal leakage points in the system both in the cylinder and the pump.

The results show that the model with the calculated leakage areas can track the experimental values at steady state. The experimental values are not smooth due to finite differentiation of potentiometer voltage to estimated piston velocity values. As described in Section 2.5, the linear potentiometer voltage data needed to be processed to obtain piston velocity and this processing caused increased noise to the signal. The velocity of the model was subject to the PID controller which caused some inconsistencies in trend being able to match the rise rate of the hardware velocity. The aim of this model was not the control loop so problems associated with it are not addressed here.

The limitation of this method for calculating leakage was assuming the measured

experimental piston velocity could be directly attributed to the flow rate into the cylinder as was done in (2.19). Because cylinder force efficiency was unknown, there is no way of separating the effect of friction on the velocity from the flow rate causing that velocity. A more complete cylinder model would include volumetric and force efficiency data in the calculation of piston velocity.

4.3 Model Validation

The recorded rod-side pressure of the prototype was compared to simulation outputs (Fig. 3.18 through 3.20). The model could represent the pressure transients of the system. The rate of pressure rise is a direct effect of system velocity along with fluid properties and friction. The heavier load reaches its steady state value later than the lighter loads. This did not match the experimental data which have the opposite with the lighter loads reaching steady state later than the heavier ones. One explanation for this is the sealing mechanism of the cylinder seals was not accounted for by not including a full cylinder force efficiency estimate in the model. The friction force of the cylinder includes many elements such as the seal preload force, breakaway friction, and coulomb friction. Practically it is difficult to separate these out and determine their coefficients; therefore a general estimate was used in the simulation that did not fully account for the particular cylinder used in the prototype. At higher loads more force could have been imparted on the seals, allowing less leakage, and causing the pressure to rise faster.

4.4 Model Exploration

Two transitions are seen in the pressure curve. The first transistion in Fig. 3.8 is the pressure needed in the cylinder to lift the load. It is when this pressure is reached that the piston begins to move. Next the pressure rises further because of the system dynamics seen in (2.9), where the velocity of the piston is dependent on the pressure in both the cap-side and the rod-side of the cylinder. The cap-side pressure builds because the flow is larger therefore more fluid volume is attempting to move at the same velocity as the rod-side flow. This causes compression of this cap-side volume and pressure there

increases and the rod-side pressure increases in response. The second shoulder seen in Fig. 3.8 is due to the check valve on the cap-side of the cylinder opening, relieving this extra flow, and pressure reaching steady state. On the cap-side this pressure is equal to the cracking pressure of the check valve. On the rod-side this pressure is found using (2.9) and the known pressure and area of the cap-side, the piston velocity, and the load force. This dependency of the rod-side pressure on the value of the cap-side pressure explains why the pressure does not immediately reach steady state and instead rises almost exponentially. To demonstrates the practical necessity of the check valve, two extremes were examined.

Looking at Fig. 3.9 and 3.10 shows the necessity of the check valves in this system. Without relieving the extra volume the fluid continues to compress and the pressure keeps rising. Having an open tank to relieve the extra flow would increase cylinder efficiency however it would not make dorsiflexion possible since the cap-side needs to be pressurized to extend the cylinder. Two solutions to this volume discrepancy are using a double-rod cylinder and using other combinations of valves. The double-rod cylinder has equal volumes on both sides since the rod extends through both sides of the cylinder, Fig. 4.1. This is not a likely solution because an extra rod in the current design would be freely moving in space.

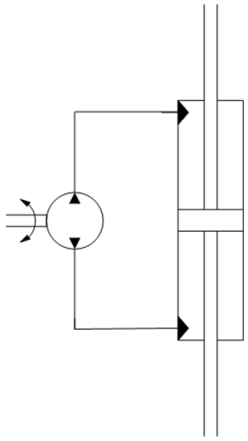

Figure 4.1: *A double-acting cylinder does not have volume difference between sides but the extra rod is not needed in this design.*

The shuttle valve in Fig. 4.2 is a three-way valve that would connect both the rod

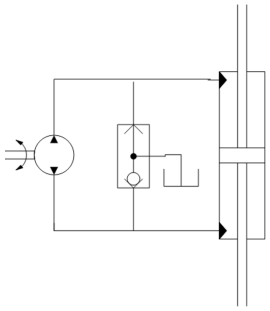

Figure 4.2: *Using a shuttle valve in the system keeps the low pressure side at reservoir pressure.*

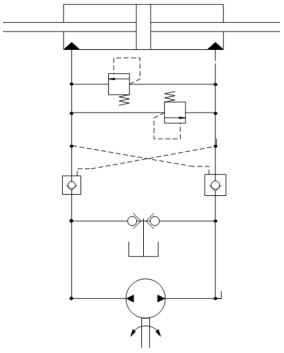

Figure 4.3: *An electrohydraulic actuator (EHA) uses a set of pilot-operated check valves for load-holding and back-to-back check valves for volume compensation. EHA are commercially available for aircraft flight control.*

and cap-sides to a tank and keeps the lower pressure side at reservoir pressure [37]. Using two back-to-back check valves or pilot-operated check valves would create a valve system that opens immediately when pressure in the rod-side builds. An example of this construction is the electrohydraulic actuator in Fig. 4.3. These valve choices are not acceptable for the current HAFO because they are only available for large flows and pressures and built into heavy manifolds that do not allow easy integration into this system. One solution being explored is integrating valves into the cylinder body to reduce weight and system complexity caused by routing separate lines to and from existing valves.

Examining the maximum requirements from the gait data, the simulation of the model has a maximum motor torque that is within the capabilities of the prototype

motor, seen in Fig. 3.21. The velocity needed to achieve maximum ankle speed is not possible with this motor. A large factor was the moment arm at the ankle was long requiring a high linear velocity at the piston to achieve the angular velocity at the ankle. The model can be used to explore different moment arm lengths as was seen in Fig. 3.2 through 3.5. More exploration of moment arms and component sizing reveals that the system can be optimized.

Efficiency of the different components is dependent on their ability to convert input power to output power effectively. Examples were given of the check valve cracking pressure and the cylinder bore diameter effecting system efficiency and how pump displacements affect system outputs. The check valve cracking pressure effects the cap-side pressure as was discussed earlier and a higher cap-side pressure means the rod-side pressure must be higher to overcome it. Pressure created to overcome losses lowers the efficiency of the system. The result of this is that if the check valve is used to relieve volume and pressure on the cap-side, it must be set to a pressure that maximizes the efficiency of the system. As seen in Fig. 3.22, a check valve setting of 50psi creates a 75% efficient cylinder. Looking at Fig. 3.3, the pressure during dorsiflexion needs to be less than 0.2 MPa or 30 psi, which would create an 85% efficient cylinder. Examing Fig. 3.23 as the bore diameter of the cylinder decreased, it became more inefficient due to the higher pressure needed on a smaller surface area to lift the load. When looking at pump sizing the pump displacement has an effect on the outputs of the pump. A higher displacement creates a larger flow rate and smaller pressure resulting in a higher cylinder velocity which could help solve the problem of the current prototype being too slow. A lower pressure means a lower torque at the motor. These are just a few of the tradeoffs that are present in this power transmission and must be taken into account during design. The simulation allows these tradeoffs to be studied and compared, but could also be used to look at different valve setups as discussed above or other pump types for examples. The flexibility of the model is the greatest advantage.

The last component in the system is the fluid that transmits power through the hydraulic circuit. The fluids properties affect the force and velocity transmission through the system. The large bulk modulus fluid is less compressible resulting in a faster rise to the pressure needed to lift the load and crack the check valve as seen in Fig. 3.25. The flow rate is also affected by the density and viscosity in Fig. 3.26. When choosing a fluid

to use in the power transmission these factors must be examined. The fluid properties of a liquid cannot be customized easily so a fluid must be chosen with an acceptable combination. For this prototype mineral oil was chosen because it was inexpensive and nontoxic. Its bulk modulus was acceptable though a stiffer fluid would have less pressure transient than was seen in these results, but not many fluids exist with a higher modulus and similar viscosity.

4.5 Design Recommendations

Based on the coupling of the components, the HAFO transmission can be designed with a variety of parameter combinations whose effects were explored with the model. The best combinations will fulfill the requirements of the HAFO; providing full ankle torque and velocity, while being lightweight, and compact.

Motors are characteristically high speed and low torque therefore combining a DC motor with a small displacement pump would result in a system with a low flow rate. A lower flow rate results in a small velocity at the ankle. This small velocity allows a small moment arm to be used. A small moment arm and low pump displacement require a higher motor torque to create the desired force at the ankle. This is the tradeoff of the transmission as power must be conserved within each component.

The model was used to make recommendations for the next design iteration. The cylinder bore diameter is set at half an inch to keep the system small and compact. Using an achievable motor speed of 6,000 rpm in combination with a pump displacement of 0.4 cc/rev results in a piston velocity of 0.2 m/s. A moment arm of 5 cm with this piston velocity achieves the desired ankle angular velocity. With a 5 cm moment arm and the half-inch diameter bore cylinder, a motor torque of 1.2 Nm is needed to achieve maximum ankle torque.

Due to this torque, the cylinder and pump will have to withstand 2,000 psi. Most hydraulic equipment is built to withstand at least 2,000 psi. A search did not find any currently available hydraulic cylinders of half-inch diameter or hydraulic piston pumps that operate at 6,000 rpm. These components would have to be customized for the system.

Chapter 5

Conclusion

5.1 General Conclusions

The design for a power transmission to drive a hydraulic-powered ankle foot orthosis was presented. The objective of this work was to develop a method to understand the design requirements of this AFO and to model the system for further analysis of components and design configurations. The HAFO developed here aimed to fill the gap in current technology by creating AFO that was powerful enough to replace ankle function while being lightweight and compact.

From this study four conclusions can be made:

- The design requirement method allows comparison component sizing but is too simplistic.
- The HAFO transmission model is representative of the "real life" prototype though expansion and refinement of the component models are needed.
- The transmission design is not the most efficient due to the design of the hydraulic circuit and the use of a single double-acting cylinder.
- To implement the recommended design, components will have to be customized.

The design requirement method worked through each component of the transmission allowing comparison of the component's sizes. The sizing determined how the power was traded off in each component. While useful for understanding these tradeoffs, the

method did not allow optimization over a range of variables and the equations did not take leakage or friction into account. This method could be expanded to add detail and allow simultaneous comparison of a range of variables for all components of the transmission.

The HAFO transmission model represented the output of the prototype and could be used to understand system behavior and efficiency. However to allow for a more complex and detailed analysis, the model could be expanded to: account for seals and friction forces in the cylinder, model the axial piston pump, and completely model the brushless DC motor with speed compensation. A more detailed model will provide increased understanding of system operation and better system design.

The realization of the transmission design incorporated a set of check valves to control the fluid volumes. The check valves were not efficient due to the need to build pressure to open them. Another design of the transmission will include back-to-back check valves that open without a significant amount of pressure and loss of efficiency. The design also specified a double-acting cylinder which necessitated the use of the check valves. If the double-acting cylinder is replaced with a double-rod cylinder, then the volume differences will be negated. Using a single-acting cylinder with spring return will simplify the system since pressure is only needed on one side. A full investigation of these alternatives will require the model to be altered.

Implementing the current transmission design per the given design recommendations will require a piston pump speed of 6,000 rpm and a system pressure of 2,000 psi. A pump of these specifications was not found in a product search and will have to be custom-made or modified from an existing design. A half-inch diameter bore cylinder that is light and compact and able to withstand high pressures will have to custom-made as well. The limited availability of compact components in a variety of operating ranges is one of the current challenges faced by hydraulic technologies.

References

[1] J. Rose and J. Gamble. *Human Walking*. Williams and Wilkins, Baltimore, MD, 2nd ed edition, 1994.

[2] D. A. Winter. *The Biomechanics and Motor Control of Human Gait: Normal, elderly and pathological*. Univ. Waterloo Press, Waterloo, ON, Canada, 1991.

[3] M. Rabuffetti R. Riener and C. Frigo. Stair ascent and descent at different inclinations. *Gait Posture*, 15(1):32–44, Feb 2002.

[4] S. Fukashiro and P. V. Komi. Joint moment and mechanical power flow of the lower limb during vertical jump. *Int J Sports Med*, 08(S 1):S15,S21, 1987.

[5] J. Perry and J. M. Burnfield. *Gait Analysis: Normal and Pathological Function*. SLACK Inc., Thorofare, NJ, 2nd ed. edition, 1992.

[6] T.M. Kepple, K.L. Siegel, and S.J. Stanhope. Relative contributions of the lower extremity joint moments to forward progression and support during gait. *Gait Posture*, 6(1):1–8, 1997.

[7] S. Whiteside. Practice analysis of certified practitioners in the disciplines of orthotics and prosthetics. Technical report, American Board for Certication in Orthotics, Prosthetics, and Pedorthics, Inc., Jan 2007.

[8] A. M. Dollar and H. Herr. Lower extremity exoskeletons and active orthoses: Challenges and state-of-the-art. *Ieee Trans. Robotics*, 24(1):144–158, Feb 2008.

[9] E. T. Hsiao-Wecksler W. K. Durfee K. A. Shorter, J. Xia and G. F. Kogler. Technologies for powered ankle-foot orthoticsystems: Possibilities and challenge. *IEEE/ASME Trans. Mechatron.*, 2011.

[10] P. Ballinger. Unusual cases: Postpolio syndrome. *Update: The Journal of Continuing Education for General Practitioners*, 57(8):774–776, November 1998.

[11] D. J. Williams-C. T. Bever L. W. Forrester R. M. Macko A. Roy, H. I. Krebs and N. Hogan. Robot-aided neurorehabilitation: A novel robot for ankle rehabilitation. *Ieee Trans. Robotics*, 25(3):569–582, Jun 2009.

[12] S. Lambert C. M. Gosselin M. Noel, B. Cantin and L. J. Bouyer. An electrohydraulic actuated ankle foot orthosis to generate force fields and to test proprioceptive reflexes during human walking. *IEEE Trans. Neural Syst. Rehabil. Eng.*, 16(4):390–399, Aug 2008.

[13] J. B. Koeneman K. Bharadwaj, T. G. Sugar. Design of a robotic gait trainer using spring over muscle actuators for ankle stroke rehabilitation. *Biomech.Eng.-Trans.ASME*, 127(6):1009–1013, Nov 2005.

[14] K. M. Chan G. Loeb F. Richmond R. Rolf K. James D. J. Weber, R. B. Stein and S.L. Chong. Bionic walkaide for correcting foot drop. *IEEE Trans. Neural Syst. Rehabil. Eng.*, 13(2):242–246, 2005.

[15] J. M. Hausdorff and H. Ring. Effects of a new radio frequency-controlled neuroprosthesis on gait symmetry and rhythmicity in patients with chronic hemiparesis. *Am J Phys Med Rehabil*, 87(1):4–13, Jan 2008.

[16] T. G. Sugar K. W. Hollander, R. Ilg and D. Herring. An efficient robotic tendon for gait assistance. *J Biomech Eng*, 128(5):788–91, Oct 2006.

[17] G.M. Pratt and M.W. Williamson. Series elastic actuators. In *IEEE Int. Conf. on Intelligent Robots and Systems.*

[18] J. A. Blaya and H. Herr. Adaptive control of a variable-impedance ankle-foot orthosis to assist drop-foot gait. *IEEE Trans. Neural Syst. Rehabil. Eng.*, 12(1):24–31, Mar 2004.

[19] J. M. Czerniecki D. P. Ferris and B. Hannaford. An ankle-foot orthosis powered by artificial pneumatic muscles. *J Appl Biomech*, 21(2):189–97, May 2005.

[20] G. S. Sawicki D. P. Ferris and A. Domingo. Powered lower limb orthoses for gait rehabilitation. *Top Spinal Cord Inj Rehabil*, 11(2):34–49, 2005.

[21] G. S. Sawicki D. P. Ferris, K. E. Gordon and A. Peethambaran. An improved powered ankle-foot orthosis using proportional myoelectric control. *Gait Posture*, 23(4):425–8, Jun 2006.

[22] E. Loth W. K. Durfee K. A. Shorter, G. F. Kogler and E. T. Hsiao-Wecksler. A portable powered ankle-foot orthosis for rehabilitation. *J Rehabil Res Dev*, 48(4):459–472, 2011.

[23] T. C. Bulea M. L. Audu J. R. Schnellenberger G. Pinault C. S. To, R. Kobetic and R. J. Triolo. Stance control knee mechanism for lower-limb support in hybrid neuroprosthesis. *J Rehabil Res Dev*, 48(7):839–50, 2011.

[24] H. Negoto T. Oshima Y. Saito, K. Kikuchi and T. Haneyoshi. Development of externally powered lower limb orthosis with bilateral-servo actuator. In *2005 IEEE 9th International Conference on Rehabilitation Robotics*, page 394399. IEEE.

[25] J. R. Schnellenberger M. L. Audu T. C. Bulea R. Gaudio G. Pinault S. Tashman R. Kobetic, C. S. To and R. J. Triolo. Development of hybrid orthosis for standing, walking, and stair climbing after spinal cord injury. *J Rehabil Res Dev*, 46(3):447–62, 2009.

[26] R. Kobetic T. C. Bulea and R. J. Triolo. Restoration of stance phase knee flexion during walking after spinal cord injury using a variable impedance orthosis. *Conf Proc IEEE Eng Med Biol Soc*, 2011:608–11, Aug 2011.

[27] R. Kobetic M. L. Audu, C. S. To and R. J. Triolo. Gait evaluation of a novel hip constraint orthosis with implication for walking in paraplegia. *IEEE Trans Neural Syst Rehabil Eng*, 18(6):610–8, Dec 2010.

[28] J.B. Andersen and T. Sinkjaer. Mobile ankle and knee perturbator. *IEEE Trans. Biomed. Eng.*, 50(10):1208–1211, Oct 2003.

[29] H. Kazerooni A. B. Zoss and A. Chu. Biomechanical design of the berkeley lower extremity exoskeleton (bleex). *IEEE Trans. Mechatron.*, 11(2):128–138, 2006.

[30] K. Pasch W. Grand A. Valiente C. J. Walsh, D. Paluska and H. Herr. Development of a lightweight, underactuated exoskeleton for load-carrying augmentation. In *Proceedings 2006 IEEE Int. Conf. on Robotics and Automation, 2006. ICRA 2006.*, pages 3485–3491.

[31] S. Kanbe H. Kawamoto and Y. Sankai. Power assist method for hal-3 estimating operator's intention based on motion information. In *The 12th IEEE International Workshop on Robot and Human Interactive Communication, 2003. Proceedings. ROMAN 2003.*, pages 67–72.

[32] K. Yamamoto. Development of power assisting suit for assisting nurse labor. *JSME Int J C-Mech Sy*, 45(3):703–711, 2002.

[33] J. E. Mitchell T. J. Withrow F. Sup, H. A. Varol and M. Goldfarb. Preliminary evaluations of a self-contained anthropomorphic transfemoral prosthesis. *IEEE/ASME Trans. Mechatron.*, 14(6), 2009.

[34] M. Berniker S. Au and H. Herr. Powered ankle-foot prosthesis to assist level-ground and stair-descent gaits. *Neural Networks*, 21(4):654–666, 2008.

[35] M. A. Holgate R. D. Bellman and T. G. Sugar. Sparky 3: Design of an active robotic ankle prosthesis with two actuated degrees of freedom using regenerative kinetics. In *2nd IEEE RAS and EMBS Int. Conf. on Biomedical Robotics and Biomechatronics, 2008.*, pages 511 – 516.

[36] J. Xia and W.K. Durfee. Analysis of small-scale hydraulic systems. *Submitted to ASME J. Mech Des*, Jan 2012.

[37] N. D. Manring. *Hydraulic Control Systems.* Wiley, Hoboken, NJ, 2005.

[38] U. Kafader. *The Selection of High Precision Micro Drives.* Maxon Academy, Sachel, Switzerland, 2011.

[39] MathWorks. Matlab R2012a SimHydraulics Documentation. `http://www.mathworks.com/help/toolbox/physmod/hydro/ref/variabledisplacementpump.html`, 2011. Accessed March 1, 2012.

[40] MathWorks. Matlab R2012a SimHydraulics Documentation. http://www.mathworks.com/help/physmod/simscape/ref/hydraulicresistivetube.html, 2011. Accessed September 24, 2012.

[41] MathWorks. Matlab R2012a SimHydraulics Documentation. http://www.mathworks.com/help/physmod/hydro/ref/hydraulicfluid.html, 2011. Accessed September 24, 2012.

[42] Parker Hannafin Oildyne Division. Catalog HY22-3101D 3/11 Compact EHA. http://divapps.parker.com/divapps/auto/windpower/pdfs/EHA%20Catalog%20US%203-11.pdf, 2011. Accessed August 31, 2012.

[43] H. Jeong. A novel performance model given by the physical dimensions of hydraulic axial piston motors: Model derivation. *J Mech Sci Technol*, 21:83–97, Jan 2007.

Appendix A

MATLAB Code for Design Requirements Method

Matlab function for calculating Equations (2.1) - (2.8), where the inputs are the Angular Velocity and Torque of the ankle and the outputs are the across and through variables of the various system components.

```
function [Cyl_Out, Cyl_In, Motor, Batt_Out, Batt_In,Cyl_Out_2, Cyl_In_2, Motor_2,
Batt_Out_2, Batt_In_2] =equations_comp(Ang_Vel, Torque)

global r_1 r_2 B nf_1 nv_1 V_p nf_2 nv_2 n_m K_M K_N n_b Ang_Vel Torque Ang

Ankle=[Torque'; Ang_Vel']';% Known Ankle Dynamics (Nm, rad/s)

   %Find Force and Velocity out of Cylinder (N,m/s)
Cyl_Out=[];
%Force(N)=Torque*100/r*cos(theta)
Cyl_Out(:,1)=(100/r_1)*Ankle(:,1);
%Linear Velocity(m/s)=radius*ang_vel/100
Cyl_Out(:,2)=(r_1/100)*Ankle(:,2);
```

```
Cyl_Out_2=[];
%Force(N)=Torque*100/r*cos(theta)
Cyl_Out_2(:,1)=(100/r_2)*Ankle(:,1);
%Linear Velocity(m/s)=radius*ang_vel/100
Cyl_Out_2(:,2)=(r_2/100)*Ankle(:,2);
%Area of the cap side (converted from inches to meters)
A_cap=pi*(B*0.0254)^2/4;

   %Find Pressure and Flowrate out of Pump into Cylinder (MPa,m^3/s)
Cyl_In=[];
%Pressure(MPa)=Force/Area/CylForceEff*1e-6
Cyl_In(:,1)=Cyl_Out(:,1)*(1/A_cap)*(1e-6)*(1/nf_1);
%Flowrate=velocity*Area/cylVolEff
Cyl_In(:,2)=Cyl_Out(:,2)*(A_cap)/nv_1;

Cyl_In_2=[];
%Pressure(MPa)=Force/Area/CylForceEff*1e-6
Cyl_In_2(:,1)=Cyl_Out_2(:,1)*(1/A_cap)*(1e-6)*(1/nf_1);
%Flowrate=velocity*Area/cylVolEff
Cyl_In_2(:,2)=Cyl_Out_2(:,2)*(A_cap)/nv_1;

   %Find torque and velocity out of motor into pump (Nm, rpm)
Motor=[];
%torque(Nm)=(Pressure*1e6)*PD/100^3/2pi/PumpForceEff
Motor(:,1)=Cyl_In(:,1)*(V_p/100^3)*(1e6)*(1/(2*pi))*(1/nf_2);
%shaft speed(rpm)=Flow/PD*100^3*60/PumpVolEff
Motor(:,2)=Cyl_In(:,2)*(100^3/V_p)*60*(1/nv_2);

Motor_2=[];
%torque(Nm)=(Pressure*1e6)*PD/100^3/2pi/PumpForceEff
Motor_2(:,1)=Cyl_In_2(:,1)*(V_p/100^3)*(1e6)*(1/(2*pi))*(1/nf_2);
%shaft speed(rpm)=Flow/PD*100^3*60/PumpVolEff
```

```
Motor_2(:,2)=Cyl_In_2(:,2)*(100^3/V_p)*60*(1/nv_2);

   %Find current and voltage out of battery into motor (A, V)
Batt_Out=[];
%Current(A)=Torque/TorqueConstant/motoreff
Batt_Out(:,1)=Motor(:,1)*(1/K_M)*1000*(1/n_m);
%Voltage(V)=speed/SpeedConstant/motoreff
Batt_Out(:,2)=Motor(:,2)*(1/K_N)*(1/n_m);

Batt_Out_2=[];
%Current(A)=Torque/TorqueConstant/motoreff
Batt_Out_2(:,1)=Motor_2(:,1)*(1/K_M)*1000*(1/n_m);
%Voltage(V)=speed/SpeedConstant/motoreff
Batt_Out_2(:,2)=Motor_2(:,2)*(1/K_N)*(1/n_m);
```

Appendix B

Model Simulation

SimHydraulics Modeling-Inputs are commanded motor speed and force at the piston. Blue objects relate to cylinder modeling.

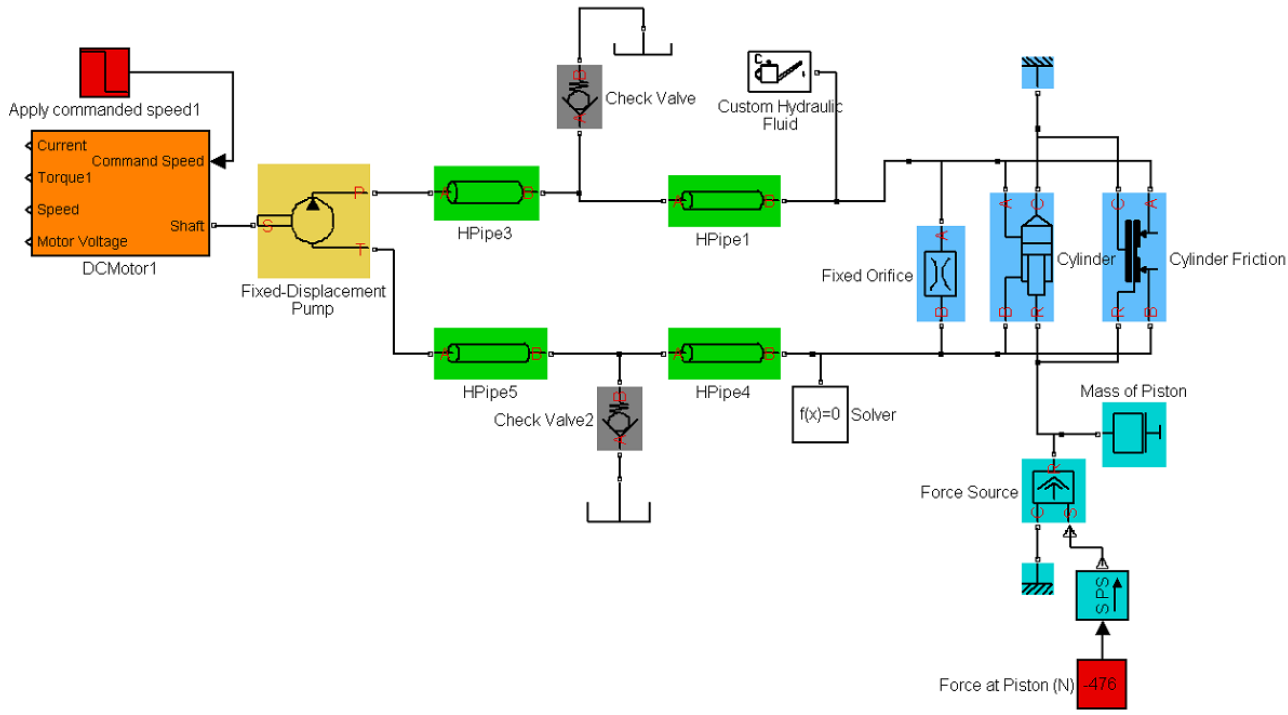

Appendix C

Datasheets

マイクロポンプ
(小型アキシアルピストンポンプ)
Micro Axial Piston Pump

TFHシリーズ／TFH-Series

手のひらサイズのTFHシリーズは世界最小クラスのアキシアルピストンポンプです。
全シリーズに球面バルブプレートを採用しており、低速から高速回転までの幅広い範囲で安定した性能を発揮します。

This palm-size TFH series is the world's smallest class of axial piston pumps.
Takako engineers have designed a spherical valve plate (SVP) concept into the entire series, creating extremely stable and highly efficient performance through a wide range of input speed.

特　長／Important Features

高性能
High performance

低速から高速回転域で性能が安定
球面バルブプレート採用
Stable performance through a wide range of output speeds.
Design incorporates a spherical valve plate design concept.

省スペース
Ergonomic

取り付けスペースに自由度がある
軽量・コンパクト
Great flexibility for application installation.
Light-weight • Compact size

高応答
Immediate Response

瞬時な正逆転の繰り返し運転が可能
rotational input can be reversed with instantaneous reaction.

基本仕様／Basic Specifications

形式 Model	押しのけ容積 Displacement	吐出圧力(MAX) operating pressure (Max.)	回転速度(MAX) Speed (Max.)	回転方向 Rotation direction	質量 Weight
	cm^3	MPa	min^{-1}		Kg
TFH-040	0.40	14	2000	両回転 Bi-directional rotational operation	0.27
TFH-080	0.80	21	3000		0.43
TFH-160	1.62				0.96
TFH-315	3.14				1.94
TFH-630	6.29				2.26

性能曲線／Performance Curve

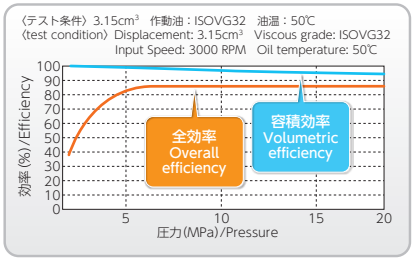

外形寸法／Dimensions

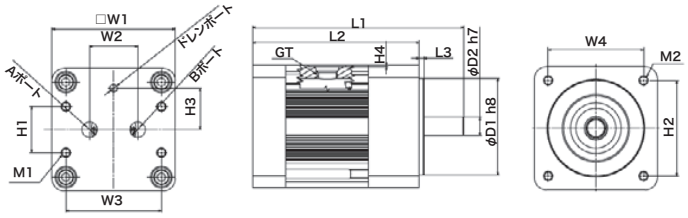

応答性グラフ／Pressure Response Graph

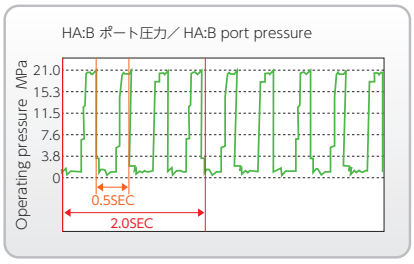

単位(㎜)/units

形式 Series	L1	L2	L3	W1	W2	W3	W4	H1	H2	H3	D1	D2	M1 M○x深さ Mounting	M2 M○x深さ Mounting
TFH-040	76.8	65	2	30	13.6	13	24	19	24	9.5	27	6	M3x6.0	M3x7.4
TFH-080	97.4	80	3	40	20.0	32	31	16	31	9.0	32	8	M4x10.0	M4x9.0
TFH-160	112.0	90	3	60	25.8	49	46	22	46	20.5	50	10	M5x12.0	M5x15.0
TFH-315	137.0	110	3	80	31.2	62	62	30	62	27.0	63	12	M6x14.0	M6x20.8
TFH-630	140.0	115	3	80	41.0	62	62	34	62	27.0	63	12	M6x14.0	M6x23.5

※ポンプ軸は、キー、Dカットタイプ　オプション対応可／Pump shaft comes with keyway or D-cut options

"500" Hydraulic Cylinders

1-1/16" Bore "500" Hydraulic Cylinders

Push Force = .886 x psi · Pull Force = .776 x psi

MODEL/PRICE	DESCRIPTION/WEIGHT (lbs.)	DIMENSIONS
H-09□-DBZ  **$69.25** *BASE PRICE* *Add $2.45 per inch of stroke*	***Front Block Mount*** *Standard Stroke Lengths:* 1", 2", 3", 4", 5", 6" Maximum Stroke – 12" *Base Weight: .57* *Adder Per Inch of Stroke: .06*	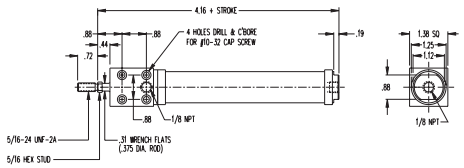
H-09□-DUZ  **$61.90** *BASE PRICE* *Add $2.45 per inch of stroke*	***Universal Mount*** *– Double End or Rear Pivot* *Standard Stroke Lengths:* 1", 2", 3", 4", 5", 6", 7", 8", 9", 10", 11", 12" Maximum Stroke – 32" *Optional Accessories:* D-8316 Mounting Bracket D-8322-A Pivot Bracket D-8309-A Clevis *Base Weight: .50* *Adder Per Inch of Stroke: .06*	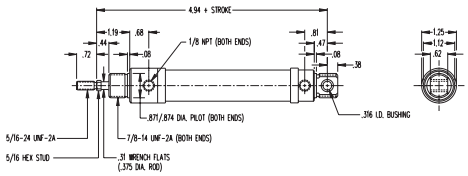
H-09□-DZ  **$56.70** *BASE PRICE* *Add $2.45 per inch of stroke*	***Nose Mount*** *Standard Stroke Lengths:* 1", 2", 3", 4", 5", 6", 7" Maximum Stroke – 12" *Optional Accessory:* D-8316 Mounting Bracket *Base Weight: .43* *Adder Per Inch of Stroke: .06*	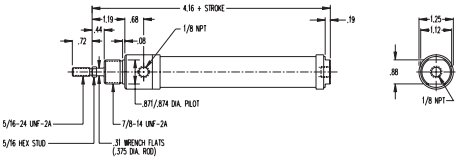

1-1/2" Bore "500" Hydraulic Cylinders

Push Force = 1.77 x psi · Pull Force = 1.57 x psi

MODEL/PRICE	DESCRIPTION/WEIGHT (lbs.)	DIMENSIONS
H-17□-DBZ  **$100.25** *BASE PRICE* *Add $3.25 per inch of stroke*	***Front Block Mount*** *Standard Stroke Lengths:* 1", 2", 3", 4", 5", 6" Maximum Stroke – 12" *Base Weight: 1.00* *Adder Per Inch of Stroke: .10*	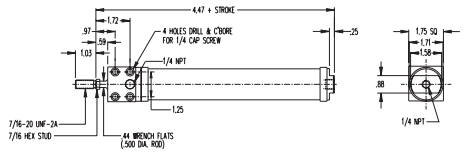

EC 45 flat brushless, 50 Watt, with integrated electronics

1-Q-speed controller

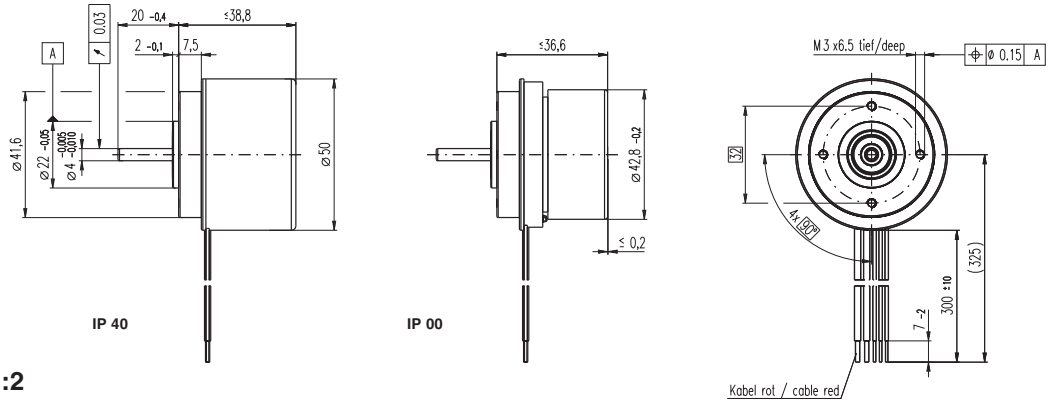

IP 40 IP 00

M 1:2

Stock program
Standard program
Special program (on request)

Order Number						
	2 wire version		5 wire version Enable		5 wire version Direction	
IP 40 (with cover)	353526		350910		370427	
IP 00 (without cover)		353524		352887		370426

Motor Data (provisional)								
	Values at nominal voltage							
1	Nominal voltage	V	24	24	24	24	24	24
2	No load speed	rpm	3000	3000	4500	4500	4500	4500
3	No load current	mA	127	127	192	192	192	192
4	Nominal speed	rpm	3000	3000	4500	4500	4500	4500
5	Nominal torque (max. continuous torque)	mNm	66	123	71	116	71	116
6	Nominal current (max. continuous current)	A	1.2	2.4	2	3	2	3
33	Max. torque	mNm	154	154	154	154	154	154
34	Max. current	A	3.3	3.3	3.8	3.8	3.8	3.8
9	Max. efficiency	%	74	74	79	79	79	79
	Characteristics							
35	Control variable		Speed	Speed	Speed	Speed	Speed	Speed
36	Supply voltage + V_{CC}	V	10 ... 28	10 ... 28	10 ... 28	10 ... 28	10 ... 28	10 ... 28
37	Speed set value input	V	= V_{CC}	= V_{CC}	0.33 ... 10.8	0.33 ... 10.8	0.33 ... 10.8	0.33 ... 10.8
38	Scale speed set value input	rpm/V	125	125	600	600	600	600
39	Speed range	rpm	1250 ... 3500	1250 ... 3500	200 ... 6480	200 ... 6480	200 ... 6480	200 ... 6480
40	Max. acceleration	rpm/s	3000	3000	6000	6000	6000	6000

Specifications

Thermal data

17	Thermal resistance housing-ambient	5.8 (2.4) K / W
18	Thermal resistance winding-housing	4 K / W
19	Thermal time constant winding	27 s
20	Thermal time constant motor	290 (116) s
21	Ambient temperature	-40 ... +85°C
22	Max. permissible winding temperature	+125°C
41	Max. temperature of electronics	+105°C

Mechanical data (preloaded ball bearings)

16	Rotor inertia		193 gcm²
24	Axial play at axial load	< 2 N	0 mm
		> 2 N	0.14 mm
25	Radial play		preloaded
26	Max. axial load (dynamic)		6.8 N
27	Max. axial load (static)		95 N
	(static, shaft supported)		1000 N
28	Max. radial loading, 7.5 mm from flange		54 N

Other specifications

31	Weight of motor	260 g
32	Direction of rotation	Clockwise (CW)

Values listed in the table are nominal.

Protective functions
Overload protection, blockage protection, inverse-polarity protection, thermal overload protection, low/high voltage cut-off

Connection 2 wire version (Cable AWG 18/24)

red	+ V_{CC} 10 ... 28 VDC
black	GND

Connection 5 wire version (Cable AWG 18/24)

red	+ V_{CC} 10 ... 28 VDC
black	GND
white	Speed set value input
green	Monitor n (6 pulses per revolution)
grey	Disable (Enable) or sense of direction change over (Direction)

Operating Range

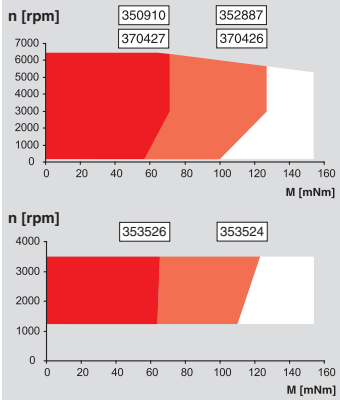

Comments

Continuous operation
The drive can be operated with a speed controller and, taking account of the given thermal resistance (fig. 17 and 18) at an ambient temperature of 25°C, does not exceed the maximum permissible operating temperatures.

Overload range
The drive reaches these operating points. Speed may vary from the set value. The overload protection shuts down the drive in the event of sustained overload.

maxon Modular System

Overview on page 16 - 21

Planetary Gearhead
∅42 mm
3 - 15 Nm
Page 240

Spur Gearhead
∅45 mm
0.5 - 2.0 Nm
Page 242